Journal of Medicinal Chemistry

Universidad de Chile

Article

The antiproliferative and uncoupling effects of delocalized, lipophilic, cationic gallic acid derivatives on cancer cell lines. Validation in Vivo in singenic mice

José A Jara, Vicente Castro, Jorge Saavedra-Olavarría, Liliana Peredo, Mario Pavani, Fabián Jaña, Maria Eugenia Letelier, María Inés Becker, Eduardo Parra, Antonio Morello, Juan Diego Maya, and Jorge Ferreira

J. Med. Chem., **Just Accepted Manuscript** • DOI: 10.1021/jm500174v • Publication Date (Web): 25 Feb 2014

The antiproliferative and uncoupling effects of delocalized, lipophilic, cationic gallic acid derivatives on cancer cell lines. Validation *in Vivo* in singenic mice.

José A. Jara,[†] Vicente Castro,[§] Jorge Saavedra-Olavarría,[§] Liliana Peredo,[†] Mario Pavanni,[†] Fabián Jaña,[†] María Eugenia Letelier,[‡] Eduardo Parra,[∥] María Inés Becker,[⊥] Antonio Morello,[†] Juan Diego Maya,[†] and Jorge Ferreira,[†,*]

[†]Clinical and Molecular Pharmacology Program, ICBM, Faculty of Medicine, Santiago, Chile.

[‡]Department of Pharmacology & Toxicological Chemistry, Faculty of Chemical & Pharmaceutical Sciences, University of Chile, Santiago, Chile.

[§]Department of Chemistry, Faculty of Basic Sciences, Metropolitan Educational Sciences University, Santiago, Chile.

[∥]Laboratory of Experimental Biomedicine, University of Tarapacá, Campus Esmeralda, Iquique, Chile.

[⊥]Development of Science & Technology Foundation (FUCITED), Santiago, Chile

Running Title: Antiproliferative and uncoupling effect of GA lipophilic cations

Keywords: lipophilic cations, mitochondriotropic, uncoupling, anticancer, gallic acid derivatives

**Corresponding author's address*: Jorge Ferreira. Clinical and Molecular Pharmacology Program, I.C.B.M., Faculty of Medicine, University of Chile. Independencia 1027, 8380453, Santiago, RM, Chile. Tel.: +56 2 9786069; Fax: +56 2 7355580

E-mail: jferreir@med.uchile.cl

Abstract

Tumor cells principally exhibit increased mitochondrial transmembrane potential ($\Delta\Psi_m$) and altered metabolic pathways. The therapeutic targeting and delivery of anticancer drugs to the mitochondria might improve treatment efficacy. Gallic acid exhibits a variety of biological activities, and its ester derivatives can induce mitochondrial dysfunction. Four alkyl-gallate triphenylphosphonium lipophilic cations were synthesized, each differing in the large of the linker chain at the cationic moiety. These derivatives were selectively cytotoxic toward tumor cells. The better compound (TPP^+C_{10}) contained 10 carbon atoms within the linker chain and exhibited an IC_{50} value of approximately 0.4 - 1.6 µM for tumor cells and a selectivity index of approximately 17-fold for tumor compared with normal cells. Consequently, its antiproliferative effect was also assessed *in vivo*. The oxygen consumption rate and NAD(P)H oxidation levels increased in the tumor cell lines (uncoupling effect), resulting in a $\Delta\Psi_m$ decrease and a consequent decrease in intracellular ATP levels. Moreover, TPP^+C_{10} significantly inhibited the growth of TA3/Ha tumors in mice. According to these results, the antineoplastic activity and safety of TPP^+C_{10} warrants further comprehensive evaluation.

Introduction

For over 60 years, propyl-, octyl- and lauryl-gallates have been permitted for use as antioxidant additives in the food and pharmaceutical industries because they have demonstrated significantly low toxicities both *in vitro* and *in vivo.*[1, 2] They act as antioxidants in a wide variety of ways, including quenching of reactive oxygen (ROS) and sulfur (RSS) species[3] and acting as potent peroxynitrite ($ONOO^-$) scavengers.[4] The reactivity of alkyl gallates toward radicals depends on the length of their alkyl chains, and their differential reactions are attributable to differences in alkyl gallate partitioning between the lipidic and aqueous pseudophases.[5-7] The intramicellar rate constants of reactions involving gallates with significantly different hydrophobicities and radicals incorporated into micelles are independent of gallate alkyl chain length.[8] The activity of alkyl gallates also includes the inhibition of several of the following pro-oxidant enzymes that are involved in the production of ROS: a) the oxidation of xantine by xantine oxidase, without inhibiting uric acid formation; b) the peroxidation of linoleic acid catalyzed by lipoxygenase-1; c) the synthesis of prostanoids and hydroxyeicosatetranoic acids catalyzed by COX-2 and 12-LOX, respectively; and d), the catalysis of superoxide dismutation into oxygen and hydrogen peroxide by superoxide dismutase.[9, 10] In addition, gallates exhibit myeloperoxidase inhibitory activity and hypochlorous acid-scavenging properties.[11] Moreover, gallates can chelate transition metal ions, such as Fe^{2+} and Cu^{2+}, which are powerful promoters of free radical damage.[10] Likewise, gallates can inhibit proreductant enzymes, such as ribonucleotide reductase, which catalyzes the rate-limiting step of *de novo* DNA

synthesis and is significantly upregulated in malignant compared with non-malignant cells.[9, 10]

Gallic acid (GA) and its ester derivatives affect the activity of a variety of both DNA and RNA animal viruses.[12-14] They elicit antimicrobial effects on Gram-positive bacteria, specifically by inhibiting the plasma membrane respiratory chain and by sensitizing antibiotic-resistant mutants to antibiotics.[15-17] Furthermore, in numerous fungal and yeast species,[3, 18, 19] gallates inhibit the mitochondrial oxidative phosphorylation system, thereby augmenting the effectiveness of fungicides.[20] Gallates not only play an important role in the prevention of inflammatory processes and malignant transformation[10] but also selectively inhibit proliferation, metastasis and anti-apoptotic and angiogenic processes. These studies have revealed considerable tumor-specific cytotoxic effects in a wide variety of human and murine tumor cell lines, such as leukemia, lung, stomach, colon, melanoma, breast, pheochromocytoma and fibrosarcoma cell lines.[4-6, 8, 21-23] In contrast, gallates prevent amyloid beta (Aβ)-induced apoptotic neuronal death.[11]

Our main interest in GA derivatives is related to their selective antitumoral activities. n-Alkyl gallates induce apoptosis in tumor cell lines predominantly by activating the mitochondria-dependent apoptotic pathway due to their association with altered mitochondrial oxidative metabolism and increased intracellular Ca^{2+} levels. n-Alkyl gallates can elicit the following effects: a) decrease mitochondrial membrane potential ($\Delta\Psi_m$); b) induce permeability transition pore opening; c) promote the release of cytochrome c, apoptosis-inducing factor (AIF), some procaspases that will be further activated and endonuclease G (Endo G); d)

upregulate the expression of Bcl-2-associated X protein (BAX) and caspase-4, caspase-9 and caspase-3 proteins, subsequently causing DNA damage and fragmentation.[21, 24] However, the mechanisms that trigger the apoptosis induced by GA and its n-alkyl ester derivatives in tumoral cells remain poorly understood. Increased concentrations of the alkyl esters of GA were first reported to elicit an uncoupling effect on the oxidative phosphorylation system, followed by an inhibition of electron flow through the respiratory chain, predominantly at the NADH-CoQ step. Both effects prevent ATP synthesis, which results in cell death. The structure and lipophilicity of the alkyl side chain of gallates are relevant for their antitumoral activities.[22]

Moreover, mitochondria play a vital role in regulating energy metabolism, cytosolic calcium concentration, ROS production and apoptosis. They exhibit significant differences in terms of the oxidative phosphorylation process between tumor and non-tumor cells; the activities of certain important enzymes involved in this process are decreased in tumor cells.[25, 26] Carcinoma cells exhibit high mitochondrial membrane potential ($\Delta\Psi_m$) and low respiration rates due to mitochondrial dysfunction.[27-29] Tumor cells also exhibit the increased expression of several proteins involved in glucose metabolism.[30, 31] In some cancer cells, aerobic glycolysis may contribute to approximately 50% of total synthesized ATP, becoming a significant source of power generation in these cells.[32] However, several studies have shown the importance of ATP production by oxidative phosphorylation in tumor cells. This process allows the direct delivery of newly synthesized ATP to the hexokinase II (HK-II) due to its interaction with the outer

mitochondrial membrane proximal to the voltage dependent anionic channel (VDAC). HK-II uses this ATP to phosphorylate and convert glucose to glucose 6-phosphate, supporting increased rates of glycolysis.[33] Furthermore, the IMM of tumor cells exhibits a $\Delta\Psi_m$ of approximately 150-180 mV; it is negatively charged on its inner face. This potential is greater than that of any other cellular organelle and that of non-tumor cells of any tissue.[28, 34] Therefore, the differences between normal and tumor cells suggest that mitochondria might represent a therapeutic target. This difference could represent a new way to circumvent the resistance to apoptotic stimuli that is exhibited by cancer cells. Considering the increased $\Delta\Psi_m$ in tumor cells, small molecules have been proposed to selectively accumulate within the mitochondria of these cells.[35] To improve the cytotoxic effects of GA esters, we synthesized different lipophilic delocalized cations gathering a GA ester with the triphenylphosphonium (TPP) moiety. The resulting compound might selectively accumulate within tumor mitochondria to elicit its cytotoxic effect, exploiting the fact that the inner mitochondrial membrane (IMM) potential differs between cancer and non-cancer cells.[27, 28] These new GA cations would bind directly to the phospholipid bilayers due to their large hydrophobic surface area, which reduces the activation energy required for the uptake of the TPP moiety.[36, 37] Because of their positive charge, these cations are driven by the potential of the cytoplasm and the mitochondrial membrane to accumulate selectively within the IMM by five hundred-fold.[37] This process would inhibit vital cellular systems by diminishing ATP synthesis and inhibiting the glycolytic pathway, which is highly dependent on the ATP produced by oxidative phosphorylation.[38] To evaluate the above statements in

this study, we assessed the cytotoxicity of the GA derivative compounds and the mechanisms through which these new molecules diminished ATP levels in tumor cells. Here, we describe the synthesis of a new cytotoxic compound that targets to mitochondria and exhibits an uncoupling action on $\Delta\Psi_m$. We further show that decreasing ATP levels is one of its principal mechanisms of inducing cell death. In addition, the most cytotoxic compound, triphenyl(10-(3,4,5-trihydroxybenzoyloxy)-decyl) phosphonium (TPP^+C_{10}), also exhibited tumor growth inhibitory activity *in vivo*. Because the mitochondria appear to represent a selective anticancer target, we determined the effect of the concentration on: i) the growth and vitality of tumour and normal cells in culture; ii) the oxidative phosphorylation process in mitochondria; iii) $\Delta\Psi_m$ generation in isolated mitochondria; iv) intracellular level of NAD(P)H/NAD(P^+) ratio; v) the opening of the mitochondrial permeability transition pore in isolated mitochondria; vi) intracellular levels of ATP, and vii) cellular death. Thus, the new molecules derived from GA may represent a new therapeutic anticancer modality cancer; their selectivity for mitochondria would minimize or avoid the adverse effects of current anticancer drugs.

Results

Synthesis of delocalized lipophilic cations of GA derivatives. The synthetic route (see methods) allowed us to derive a series of lipophilic cations that differed in the number of carbon atoms in the alkyl chains between the GA and triphenyl phosphonium moieties (Figure 1A).

Cytotoxicity of delocalized lipophilic cations of GA derivatives. The most potent cytotoxic activity on both mouse mammary adenocarcinoma (both sensitive

and resistant to chemotherapy) and human leukemia cells was exhibited by TPP^+C_{10} (Figures 1B, C and D; Table 1). The IC_{50} values obtained from the concentration response curves (as Figures 1B and C) showed that GA and triphenylphosphane (Ph3P) were the less cytotoxic. As expected, the GA conversion in ester derivatives conferred to the resulting compound greater cytotoxicity, which was dependent on the length of the hydrocarbon side chain. As well, as we supposed, the new delocalized lipophilic cationic derivative by conjugation of respective ester of GA with Ph3P showed higher cytotoxic activity. Among the group of alkyl-gallate triphenylphosphonium lipophilic cations, the derivative with the fewest carbon atoms (TPP^+C_8) was the less cytotoxic (Table 1). Strikingly, the derivative with 11 carbon atoms (TPP^+C_{11}) was less cytotoxic than TPP^+C_{10} and TPP^+C_{12}, suggesting that an odd number of carbons can hinder proper interaction with the IMM. However, further experiments are necessary to confirm this hypothesis (Table 1).

Comparisons of the IC_{50} values between tumor and non-tumor cells from the mouse mammary epithelium revealed that TPP^+C_{10} was the most selective compound of the series, with a selectivity of approximately 17-fold. Therefore, the TPP^+C_{10} derivative is more cytotoxic to tumor cells than non-tumoral cells. These results suggest that the mechanism of cytotoxicity might be related either to the perturbation of the negative membrane charge exerted by the cations or to the degree to which the compounds intercalate into the IMM. Indeed, the latter mechanism would explain the differences observed between the compounds in this series. Furthermore, although the TPP^+C_{12} compound proved to be highly cytotoxic to tumor cells, it was also toxic to non-tumoral cells and is therefore not a suitable

anticancer drug candidate. The TPP^+C_{10} compound, however, exhibited tumor cell-selective cytotoxicity.

Uncoupling effect of GA derivatives. Figure 2A shows representative traces of oxygen consumption by isolated TA3/Ha mitochondria recorded using a Clark oxygen-sensitive electrode. During glutamate plus malate oxidation in the absence of ADP, the mitochondrial respiration rate was low, but its rate was abruptly increased after the addition of ADP (State 3). This stimulation was transient, and the respiration rate spontaneously declined and remained low again (State 4). We found that the amount of oxygen consumed during this accelerated respiration phase was stoichiometrically correlated with the amount of ADP added (ADP/O = 2.3 in this example) and depended on the nature of the oxidized respiratory substrate, indicating that mitochondrial respiration is coupled to ADP phosphorylation. The added ADP was phosphorylated in parallel with stimulated respiration, and the synthesized ATP accumulated in the mitochondrial suspension. These transitions in respiration rate repeated several times until the mitochondrial suspension became anaerobic. Afterward, the ATP synthase inhibitor oligomycin was added to the same mitochondrial suspension in State 4, and we did not observe the abruptly increased oxygen consumption rate after the addition of ADP (State 3 inhibition). Subsequently, the addition of TPP^+C_8 induced an abrupt and permanent increase in respiration until the oxygen concentration was exhausted (trace a), and this increase was inhibited by cyanide (trace b). Consequently, TPP^+C_8 exhibited features of an uncoupler because it stimulated oxygen consumption with a consequent decrease in the $\Delta\mu H^+$ caused by energy dissipation and without a concomitant increase in the ATP synthesis.

Figure 2B shows the result of titrating respiration with TPP^+C_8. Similar to conventional uncouplers, such as carbonyl cyanide *m*-chlorophenyl hydrazone (CCCP) or carbonyl cyanide *p*-trifluoromethoxyphenylhydrazone (FCCP) [39], respiration was markedly stimulated by 10^{-4} M TPP^+C_8 and increased proportionally as the concentration was increased up to 6-fold. GA esters represent conventional but weak uncouplers [22]. They are lipid-soluble molecules, but the pKs of their phenol groups are relatively high (pK = 8.1-12.9). Consequently, the uncoupling activity is limited by low concentrations of the anionic forms.

We observed increased oxygen consumption rates in mouse mammary adenocarcinoma cells, which indicate that these cations essentially behave as uncoupling agents (Figure 2C). All the cations exhibited an uncoupling effect on the TA3/Ha and TA3-MTX-R cell lines which was comparable to the effect exerted by the classical uncouplers we used as control. The derivative with the fewest carbon atoms (TPP^+C_8) was the least potent ($K_{0.5} \approx 2 \times 10^{-4}$ M). This figure also shows the conventional behavior exhibited by TPP^+C_{12}; doubling the concentration of the cations approximately doubled their respective uncoupling effects. Thus, a plot log change in respiration rate versus log cation concentration was delineated by a straight line with a slope of approximately 1. We further plotted the observed respiration rate at each cation concentration after the addition of an excess of FCCP (full uncoupling). These results showed that the cations elicited no confounding effect on maximum respiratory capacity. The dynamic range of the concentrations from the lowest measured uncoupling to the maximum uncoupling was approximately 10 (n = 1.0). Similar results were previously reported by Lou et al.[39] for the classic uncouplers CCCP and DNP (2,4-dinitrophenol). Interestingly,

TPP^+C_{10} can be considered a relatively safer uncoupler because its uncoupling effect increased gradually as its concentration increased (the slope in log-log plot was approximately 0.42 - 0.54), thereby widening the distance between therapeutic and toxic doses and providing a therapeutic range of approximately 500-fold. Moreover, uncoupling by TPP^+C_{10} at concentrations below 10^{-5} M was only completely inhibited by atractyloside, and the slopes of the log-log plots were steeper ($n \approx 1.0$), suggesting that uncoupling at these concentrations required adenine nucleotide translocase activity.[39]

Intracellular ATP content. The uncoupling effect induced by the GA derivatives is expected to result in decreased intracellular ATP content. We therefore evaluated the effect of acute exposure to these compounds. The results are shown in Figure 3. For all compounds, the ATP levels decreased significantly in the TA3/Ha cell line (Figure 3); TPP^+C_{10} (Figure 3B) and TPP^+C_{12} (Figure 3D) were the more potent compounds, and TPP^+C_8 (Figure 3A) and TPP^+C_{11} (Figure 3C) were the weaker compounds. Moreover, decreased ATP levels occurred in a concentration-dependent manner. This decrease was not due to cell death; at the concentration range tested, the percentage of cell death was relatively small compared with the decrease in ATP content (Figure 3E).

Metabolic state of TA3/Ha tumor cells. To assess the metabolic state of mitochondria in tumor cells, we studied the oxidation of reduced nicotinamide adenine nucleotide (NAD(P)H). The oxidative transition state was evaluated by measuring the metabolic NAD(P)H/$NAD(P)^+$ ratio. Rotenone is a known inhibitor of NADH oxidation; it increases the relative NAD(P)H/$NAD(P)^+$ ratio (reduced state). Accordingly, the addition of 12 μM rotenone increased NAD(P)H auto-fluorescence

(Figure 4A). The transition is consistent with increased NAD(P)H levels as a result of the inhibitory effect of rotenone on electron flow. To decrease the NAD(P)H/NAD(P)$^+$ ratio (i.e., to favor NAD(P)H oxidation), an uncoupler might be added to the mitochondrial preparation. FCCP is a classical electron transport chain uncoupler that increases electron flow and favors the oxidation of NAD(P)H, thereby decreasing the NAD(P)H/NAD(P)$^+$ ratio. Relative to untreated mitochondria, the addition of 6 µM FCCP decreased the auto-fluorescence of NAD(P)H, thus decreasing NAD(P)H levels, which is consistent with its known uncoupling properties (Figure 4A). The addition of the most cytotoxic cationic derivative (TPP^+C_{10}) to the mitochondrial preparation produced a similar effect as that observed with FCCP (i.e., decreased NAD(P)H auto-fluorescence) and was dependent on the concentration of TPP^+C_{10}. Therefore, these results suggest that TPP^+C_{10} promotes the oxidation of NAD(P)H and the reduction in the NAD(P)H/NAD(P)$^+$ ratio.

$\Delta\Psi_m$ decrease produced by TPP^+C_{10}. Decreased $\Delta\Psi_m$ is widely used as an early measure of cell death. This parameter was evaluated using the lipophilic cations safranin and JC-1. These results showed that upon the addition of TPP^+C_{10} to mitochondria isolated from TA3/Ha cells, the $\Delta\Psi_m$ decreased sharply in a manner comparable to that exerted by CCCP (Figures 4C and D). The same effect was observed when testing TPP^+C_{10} on TA3/Ha cells treated with JC-1 (Figure 4E). Unlike the expenditure of $\Delta\Psi_m$ when ATP is synthesized, the level of $\Delta\Psi_m$ apparently remained constant (Figure 4B) due to compensation by an increased respiration rate (Figure 2A). This effect occurred early in tumor cells exposed to

TPP^+C_{10}, suggesting that it plays a pivotal role in cell death triggered by this GA derivative.

Regulation of the mitochondrial permeability transition pore (mPTP). Figure 5A shows an increase in mitochondrial swelling proportional to the concentration of TPP^+C_{10} on both TA3/Ha cells and their multidrug resistant variant (TA3-MTX-.R). However, this phenomenon was not completely reversed by the classical inhibitor of this process, cyclosporine A (CsA) (Figure 5B). Furthermore, the mitochondrial swelling was partially reversed by protective molecules from the oxidation of sulfhydryl groups present in adenine nucleotide translocase (ANT), such as NEM (Figure 5C), DTT (Figure 5D) and NAC (Figure 5E). These data suggest that the GA derivatives previously oxidized in the respiratory chain might interact with the sulfhydryl groups present in ANT, thereby regulating the opening of the mPTP.

GA derivatives induce cell death. Early and late apoptosis and necrosis were expressed as the percentage of Annexin-V+/PI-, Annexin-V+/PI+ and Annexin-V-/PI+ cells, respectively.[40] In Figure 6A, we evaluated the activation of caspase 3 at concentrations near the IC_{50} for TPP^+C_{10}. We observed that this compound activated caspase 3, whereas the other derivatives, which are less potent, did not and required higher concentrations to elicit the same effect. Furthermore, TPP^+C_{10} induced a cell cycle arrest in G_0/G_1 phase, which is a characteristic effect of uncouplers (Figure 6B). Figures 6C through 6F show that cells treated with GA derivatives are primarily in the early stages of apoptosis at 24 and 48 h, and the most potent compound was TPP^+C_{10}. We also found that the percentage of PI-permeable cells was negligible, indicating that necrosis is irrelevant as the type of

cell death induced by these lipophilic cations. These phenomena are consistent with the low lactate dehydrogenase activity observed in Figure 6G.

TPP^+C_{10} induces antitumor effects in a syngenic model of TA3/Ha-derived tumors. We examined the inhibitory effect of TPP^+C_{10} on tumor growth *in vivo* using a well-established syngenic tumor mouse model.[41, 42] This model consists of the inoculation of tumor cells of the same species as the recipient animal and has the advantage that the tumor grows in an immunocompetent host.

A dose of 10 mg of TPP^+C_{10}/kg or vehicle via i.p. every 48 h for 30 days resulted in a survival rate of mice without significant differences compared with the control group. This dose significantly inhibited tumor growth in CAF1-Jax mice compared with the control group during the treatment period (Figures 7A and B), without apparent signs of toxicity (data not shown).

DISCUSSION

Currently, extensive effort is focused on obtaining, isolating and synthesizing new compounds that inhibit pathways involved in energy metabolism in tumor cells.[43] The emphasis on tumor cell metabolism is primarily due to specific metabolic changes that occur that allow tumor cells to evade the immune response and chemotherapeutic treatments.[44] Here, we chemically modified GA, a well-known herbal antioxidant with various biological activities. The chemical modifications were designed to produce mitochondria-targeted molecules that were selectively toxic to tumor cells.[45, 46] The proposed synthetic route allowed us to obtain molecules that were linked to triphenylphosphonium, a chemical group that drives mitochondrial uptake by exploiting the charge differences of the inner and

outer faces of the IMM.[37] The negative charge of the inner face attracts cations towards the matrix, and despite its charge, cations can cross the cell membrane easily because of their lipophilicity.[36]. We designed these new molecules to identify new cancer-selective drugs that can inhibit ATP synthesis and the subsequent phosphorylation of glucose by HK-II in tumor cells. The GA ester derivatives that we synthesized have different chain lengths between the polyhydroxybenzene and TPP moieties. The design of these molecules with different chain lengths meet the need of evaluating a suitable chain length to allow a better intercalation of the cationic compounds in the inner mitochondrial membrane, since various authors have assays a set of GA esters with different lengths chain as antibacterial, antifungal or antiviral action. There are also data showing that in general the esters with less than 8 carbon atoms are less potent, as well as those with a total of close to 15 carbons are highly toxic and nonspecific. [7, 18] Thus, differences in compound efficacy depended on the length of the alkyl side chain. Perhaps both or more important than compound size, it is its shape, because it give the possibility to have some affinity degree with proteins of some inner membrane transport system. TPP^+C_{10} was the most cytotoxic and selective. It may be considered a relatively safer uncoupler because its uncoupling effect increased gradually as its concentration increased (Figure 2C), thereby widening the distance between therapeutic and toxic doses and providing a therapeutic range of approximately 500-fold. Moreover, only for the uncoupling by TPP^+C_{10} at concentrations below 10^{-5} M was completely inhibited by atractyloside, suggesting that uncoupling at these concentrations required adenine nucleotide translocase activity.[39] TPP^+C_8 was the less cytotoxic. Despite exhibiting similar toxicity as TPP^+C_{10}, TPP^+C_{12} was

significantly less selective, exhibiting similar IC_{50} values for tumor and non-tumor cells. Therefore, the low selectivity of TPP^+C_{12} is likely to result in adverse effects. Thus, further experiments are necessary for evaluating the toxicity of TPP^+C_{12} in human cells and in animals. Indeed, tumor cell specificity remains one of the most critical issues in the search for new anticancer drugs.

All the compounds tested increased oxygen consumption in the presence of oligomycin, indicating that at the concentrations tested, all the derivatives are uncouplers. This effect is different from that observed for GA esters that lack the triphenylphosphonium moiety because these molecules act as inhibitors of electron flow through the respiratory chain in tumor cells.

Consistent with the mechanism of action of these compounds on mitochondrial metabolism, rotenone and FCCP induced changes in the auto-fluorescence of NAD(P)H. In mitochondria of TA3/Ha cells, the most potent compound (TPP^+C_{10}) induced a concentration-dependent decrease in the NAD(P)H/$NAD(P)^+$ ratio (a similar effect to that produced by FCCP), indicating that the electron transport chain was actively using NADH as an electron donor.[47] Furthermore, the availability of NADPH is relevant in the process of GSH recovery via glutathione reductase and thioredoxin regeneration through the action of thioredoxin reductase, among other critical processes for the tumor cell. [48]

The uncoupling effect elicited by these new molecules also decreased the ATP synthesis that is coupled to the oxidative phosphorylation system. This decrease might occur, for example, via a decrease in glucose phosphorylation catalyzed by HK-II, leading to decreased glycolytic flow. HK-II is a large isoenzyme that is over-expressed in many tumor cells and is crucial for the glycolytic

pathway.[43, 49] The uncoupling effect can be achieved through a variety of mechanisms. For example, uncoupling can occur as a result of the neutralization of a negative charge located on the inner face of the IMM by positively charged cations (i.e., potential-sensitive uncoupling effect). Another possible mechanism is the delivery of protons into the mitochondrial matrix and the subsequent recruitment of anionic species by ANT. Next, compounds might interact near ANT, capturing a proton from the intermembrane space and transferring it back to the mitochondrial matrix, acting as a proton shuttle from the intermembrane space into the matrix. This mechanism is facilitated by the interaction of the molecules with ANT. Many studies have reported that conventional uncoupling, such as that observed in DNP-induced apoptosis of Calu-6 lung cancer cells, can occur as a result of the production of ROS production, cell cycle arrest in G1 phase and a decrease of reduced glutathione levels.[50] The uncoupler FCCP also inhibits the growth of Calu-6 cells through apoptosis and cell cycle arrest by decreasing cyclin-dependent kinase (CDK) and activating caspases, respectively. A close relationship between the uncoupling effect, decreased reduced glutathione levels and the ability of these compounds to trigger cell death has also been suggested.[50]

Furthermore, protonated weak lipophilic acids of aromatic compounds can augment the H^+-permeability of the IMM by facilitating H^+ transport across the hydrophobic barrier. Many other mechanisms that increase mitochondrial H^+ conductance have been described, including the following: a) H^+ leakage via different uncoupling proteins (UCPs), which is inhibited by GDP; b) allosteric stimulation by AMP on H^+ leakage through ANT, which is inhibited by atractyloside and derivatives; c) the transmembrane cycling of protonated/deprotonated free

fatty acids; and d) a H^+ sub-conductance state of the mPTP. These mechanisms might be activated by various events that induce mitochondrial dysfunction, including ROS generation, PTP opening or increases in AMP concentration. However, whether increased H^+ conductance plays a deleterious or protective role in terms of cellular viability remains poorly understood.[51]

In contrast, the mitochondrial swelling assay revealed that the compounds can induce the opening of the mPTP. This effect was not reversed by the classical inhibitor CsA. However, redox-active molecules, which avoid thiolic group oxidation, partially reversed the opening of the mPTP (Figure 5). As a consequence, partially oxidized GA appeared to be able to interact with the protein sulfhydryl groups present in ANT. This interaction could result in a permanent stimulation of mPTP opening—a hypothesis that remains to be studied.[52, 53]

Furthermore, we assume that the GA ester derivatives bound to the TPP group would exhibit improved cytotoxic activity with low IC_{50} values. They exhibit an important selectivity toward tumor cells, causing mitochondrial dysfunction, which results in severely decreased $\Delta\Psi_m$ and intracellular ATP levels. Both of these effects are potent triggers of mitochondria-mediated cell death, leading to the release of classical mitochondrial proteins, such as cytochrome c, apoptosis-inducing factor, endonuclease G, Smac/DIABLO and Omi/HtrA2, which lead to apoptotic or necrotic cell death.[54-57]

Furthermore, these decreases exert a strong signal to inhibit cellular proliferation and to activate the death machinery, as reflected in a concentration-dependent accumulation of cells in G_1 phase and in the activation of caspase 3

observed approximately at the IC_{50} values of TPP^+C_{10}. The death induced by these derivatives was principally apoptosis. This effect is reflected by the exposition of PS, the low rate of PI incorporation and LDH activity. The effects listed above suggest that targeting of GA to the mitochondria of tumor cells through the TPP moiety does not modify the pharmacologic mode of action of GA.

Nonetheless, preliminary experiments in animal models have yielded promising results. At a concentration of 10 mg/kg body weight, treated mice group exhibited a statistically similar survival curve compared with the control group. Furthermore, the final volumes of the TA3/Ha tumors were significantly lower than those of the control group at 25 days after the i.p. administration of TPP^+C_{10} (Figure 7B). Interestingly, a preclinical study performed with tetradecyl gallate reported a decrease in tumor size and metastasis of melanoma in an animal model. According to the authors, this effect was attributed to the inhibition of GSH synthesis and to the depletion of ATP, with no apparent signs of toxicity.[58] Therefore, further experiments are underway to evaluate the toxicity and effectiveness of these compounds as potential anti-neoplastic cancer agents[59].

Conclusion

Extensive studies have reported on the diverse range of effects of both GA and its esters. Most of these reports describe the increase of oxidized glutathione levels as a primary cause of cytotoxicity against various cell types, including tumor cells. Through this mechanism, most of these reports have attributed the cytotoxicity to the ability of GA to produce free oxygen radicals. The production of ROS can exert a variety of deleterious effects at the intracellular level. For this reason, we chemically modified the GA derivatives to improve their activity and selectivity.

Moreover, we propose a primary mechanism of action that targets the highly conserved $\Delta\Psi_m$ and that consequently reduces ATP synthesis by the oxidative phosphorylation system, which is essential for sustaining the metabolic reprogramming exhibited by tumor cells. The mechanism of action described for these lipophilic cations is consistent with most of the effects that characterize GA and esters. We consider that the effects described by previous studies occur downstream of the decreased synthesis of ATP. Furthermore, there are many examples of the use of lipophilic cations to drive molecules, mainly antioxidant to mitochondria. It is so far we can only find molecules with antioxidant activity mainly[59-62]. However, in this work we shown that this strategy is used to selectively deliver cytotoxic molecules to mitochondria in order to disrupt the mitochondrial functioning in tumor cells both *in vivo* and *in vitro*.

Experimental section

Materials.

Atractyloside (ATC), bovine serum albumin (BSA), CCCP, FCCP, cyclosporine A, dichlorofluorescein diacetate, digitonin, Dulbecco's modified Eagle's medium (DMEM), fetal bovine serum (FBS), glutamate, glutamine, malate, neutral red, oligomycin, propidium iodide (PI), RPMI 1640 culture medium, triton X-100, trypan blue 0.4% solution, primary antibodies for β-tubulin and succinate were purchased from Sigma Chemical Co. (St. Louis, MO, USA). The primary antibodies for caspases 3 were purchased from Cell Signaling Technology (Boston, MA, USA). All other organic compounds and inorganic salts, acids and solvents were purchased from Merck (Darmstadt, Germany) unless otherwise specified. All

reagents and solvents used for the synthesis of the derivatives were purchased from Sigma-Aldrich (St. Louis, MO, USA) or Merck (Darmstadt, Germany) and were used without further purification.

General Experimental Procedures.

We recorded the ^{1}H and ^{13}C nuclear magnetic resonance (NMR) spectra using a Bruker Avance 400 spectrometer equipped with a Bruker inverse 5-mm Z gradient probe operating at 400.13 MHz and 100.62 MHz, respectively. All experiments were conducted at a probe temperature of 300 K using solutions in DMSO-d_6 with tetramethylsilane (TMS) as an internal standard. The chemical shifts are reported as δ (ppm) downfield from TMS for ^{1}H NMR. Coupling constants (J) are presented as Hz. Electron image mass spectroscopy was run on a Thermo Finnigan MAT 95XP instrument with electron impact ionization at 70 eV and perfluorokerosene as a reference. Elemental analyses were performed using a Fisons Carlo Erba EA1108 Elemental Analyzer; values were within ±0.5% of the calculated values. Consequently, these compounds meet the criteria of >95% purity, which showed good *in vitro* and *in vivo* activity.

Synthesis of (8-hydroxyoctyl)triphenylphosphonium bromide (1). A solution of 8-bromooctan-1-ol (244 mg, 1.16 mmol) in dry acetonitrile (100 ml) was treated with triphenylphosphine (310 mg, 1.18 mmol). The solution was refluxed with stirring for 48 h. The solvent was removed in a vacuum, and the crude product was subjected to chromatography on silica gel (EtOAc, MeOH) to yield compound **1** as a colorless oil (384 mg, 70%). ^{1}H NMR (400 MHz, DMSO-d_6): δ 1.12-1.51 (m, 14H, CH_2), 3.57 (t, J = 6.8 Hz, 2H, CH_2), 7.73-7.91 (m, 15H, ArH), HRMS *m/z* 470.1041 (calculated for $C_{26}H_{32}BrOP$, 470.1374).

Synthesis of (10-hydroxydecyl)triphenylphosphonium bromide (2). Following the same procedure as described for obtaining compound **1**, we synthesized compound **2** as a colorless oil (1.2 g, 63%). ^{1}H NMR (400 MHz, DMSO-d_6): δ 1.01-1.51 (m, 18H, CH_2), 3.57 (t, J = 7.1 Hz, 2H, CH_2), 7.73-7.91 (m, 15H, ArH), HRMS *m/z* 485.4312 (calculated for $C_{27}H_{33}BrOP$, 485.4357).

Synthesis of (11-hydroxyundecyl)triphenylphosphonium bromide (3). Following the same procedure as described for obtaining compound **1**, we synthesized compound **3** as a colorless oil (230 mg, 31%). ^{1}H NMR (400 MHz, DMSO-d_6): δ 1.13-1.64 (m, 20H, CH_2), 3.32 (t, J = 6.6 Hz, 2H, CH_2), 7.72-7.88 (m, 15H, ArH), HRMS *m/z* 512.0890 (calculated for $C_{29}H_{38}BrOP$, 512.1843).

Synthesis of (12-hydroxydodecyl)triphenylphosphonium bromide (4). Following the same procedure as described for obtaining compound **1**, we synthesized compound **4** as a colorless oil (242 mg, 53%). ^{1}H NMR (400 MHz, DMSO-d_6): δ 1.18-1.59 (m, 20H, CH_2), 3.34 (t, J = 6.4 Hz, 2H, CH_2), 7.50-7.90 (m, 15H, ArH), HRMS *m/z* 527.5061 (calculated for $C_{30}H_{40}BrOP$, 527.5152).

Synthesis of triphenyl(8-(3,4,5-trihydroxybenzoyloxy)octyl)phosphonium bromide *($TPP^+C_8Br^-$).* In an atmosphere of N_2, a solution of GA (225 mg, 1.3 mmol) in dry dimethylformamide (DMF) (50 ml) was treated with a solution of N,N-dicyclohexylcarbodiimide (DCC, 272 mg, 1.3 mmol) in dry DMF (30 ml). The mixture was cooled to 0℃, and a solution of (8-hydroxyoctyl)triphenylphosphonium bromide (**1**, 520 mg, 1.1 mmol) in DMF (10 ml) and N,N-dimethylpyridin-4-amine (DMAP, in catalytic amounts) in DMF (5.0 ml) was added. The reaction was stopped the next day, and any resulting precipitate was removed by filtering. The solvent was then removed, producing a brown residue that was subjected to

chromatography on silica gel (DCM, MeOH) to yield compound **5** as a light yellow oil (282 mg, 41%). ^{1}H NMR (400 MHz, DMSO-d_6): δ 1.17-1.55 (m, 14H, CH_2), 3.55 (t, J = 6.5 Hz, 2H, CH_2), 6.92 (s, 2H, ArH), 7.75-7.88 (m, 15H, ArH); HRMS *m/z* 622.0301 (calculated for $C_{33}H_{36}BrO_5P$, 622.1487).

Synthesis of triphenyl(10-(3,4,5-trihydroxybenzoyloxy)decyl)phosphonium bromide *(TPP$^+$C$_{10}$Br$^-$).* Following the same procedure as described above for obtaining ***TPP$^+$C$_8$Br$^-$***, we synthesized ***TPP$^+$C$_{10}$Br$^-$*** as a light yellow oil (701 mg, 36%). ^{1}H NMR (400 MHz, DMSO-d_6): δ 1.18-1.52 (m, 18H, CH_2), 3.53 (t, J = 6.3 Hz, 2H, CH_2), 6.92 (s, 2H, ArH), 7.72-7.88 (m, 15H, ArH); ^{13}C NMR (DMSO-d_6) δ 20.24, 20.74, 22.08, 25.82, 28.45, 29.00, 29.22, 30.19, 32.82, 61.04, 109.14, 118.50, 119.34, 125.41, 130.52-130.65 (m), 133.86-133.96 (m), 135.22 (m), 141.15, 145.76, 169.44 (CO); HRMS *m/z* 650.1109 (calculated for $C_{35}H_{40}BrO_5P$, 650.1797).

Synthesis of triphenyl(11-(3,4,5-trihydroxybenzoyloxy)undecyl)phosphonium bromide *(TPP$^+$C$_{11}$Br$^-$).* Following the same procedure as described for obtaining ***TPP$^+$C$_8$Br$^-$***, we synthesized ***TPP$^+$C$_{11}$Br$^-$*** as a light yellow oil (581 mg, 44%). ^{1}H NMR (400 MHz, DMSO-d_6): δ 1.18-1.56 (m, 20H, CH_2), 3.63 (t, J = 6.1 Hz, 2H, CH_2), 6.99 (s, 2H, ArH), 7.70-7.89 (m, 15H, ArH); ^{13}C NMR (DMSO-d_6) δ 20.21, 20.72, 22.09, 24.74, 25.83, 28.45, 29.03, 29.27, 32.83, 33.65, 61.05, 109.21, 118.48, 119.33, 130.09, 130.52-130.65 (m), 133.85-133.95 (m), 136.80 (m), 137.09, 145.73, 170.03 (CO); HRMS *m/z* 664.1632 (calculated for $C_{36}H_{42}BrO_5P$, 664.1953).

Synthesis of triphenyl(12-(3,4,5-trihydroxybenzoyloxy)dodecyl)phosphonium bromide *(TPP$^+$C$_{12}$Br$^-$).* Following the same procedure as described for obtaining

TPP$^+$C$_8$Br$^-$, we synthesized ***TPP$^+$C$_{12}$Br$^-$*** as a light yellow oil (818 mg, 39%). ^{1}H NMR (400 MHz, DMSO-d_6): δ 1.16-1.56 (m, 22H, CH_2), 3.64 (t, J = 6.6 Hz, 2H, CH_2), 6.95 (s, 2H, ArH), 7.76-7.88 (m, 15H, ArH); ^{13}C NMR (DMSO-d_6) δ 19.87, 20.37, 21.67, 25.19, 25.43, 28.06, 28.62, 29.61, 29.77, 32.44, 33.89, 61.61, 108.80, 118.11, 118.96, 120.70, 130.09-130.21 (m), 133.47-133.57 (m), 134.79 (m), 137.83, 145.42, 167.62 (CO); HRMS *m/z* 678.1967 (calculated for $C_{37}H_{44}BrO_5P$, 678.2110).

Cell lines and cell culture. The mouse mammary adenocarcinoma TA3/Ha cell line was kindly provided by Dr. Gasic, University of Pennsylvania, and has been used by our laboratory since 1989.[63] Its multiresistant variant, TA3-MTX-R, was generated under the same conditions as previously described.[64] This cell line exhibits MTX resistance and cross-resistance to CPT, DOX, 5-fluorouracil and vinblastine.[64] Both cell lines were propagated until the day of the assay by weekly i.p. inoculation of ascitic fluid into young adult male CAF1/J mice and harvested after 5-7 days as described previously.[64] The mice were purchased from the animal facility of the Faculty of Medicine of the University of Chile, where they were housed and fed under the same conditions as previously described.[64] The University of Chile Committee on Animal Welfare and CONICYT approved all the animal protocols used in this study, and all precautions were taken to ensure that the animals did not suffer unduly. The murine tumor cells and epithelial mammary gland cell line MM3MG (ATCC, Catalogue No. CRL-6376, Manassas, VA) were cultured in DMEM supplemented with 10% inactivated fetal calf serum (FCS) and 1% antibiotics (penicillin/streptomycin) in a humidified atmosphere (37℃ and 5% CO_2). The human acute lymphoblastic leukemia cell line CCRF-CEM (ATCC,

Catalogue No. CCL-119) was maintained in RPMI-1640 culture medium with 10% inactivated FCS and 1% antibiotics under the same conditions as described above.

Mitochondrial preparation. Mitochondrial suspensions of approximately 40-50 mg protein/ml were prepared from the tumor cells as described previously[64, 65] with the following modifications: the mitochondrial fractions were washed twice, centrifuged at 12,000 × *g* for 10 min and re-suspended in a minimal volume of their respective medium in the absence of BSA to eliminate hydrophobic compound adsorption. Protein concentrations were determined by the Lowry reaction, and the results were standardized with serum albumin.[66]

Cellular viability assay using neutral red. The viability of the cell lines treated with different concentrations of each triphenylphosphonium lipophilic cation was analyzed using the neutral red test as previously described.[67] The test conditions were 1 × 10^5 cells/ml for TA3, TA3-MTX-R and CCRF-CEM cells and 4 × 10^4 cells/ml for MM3MG cells. The tumor cells were grown in 96-well tissue plates in a humidified atmosphere at 37°C and 5% CO_2 for 48 h in the absence (controls) or presence of different concentrations of the lipophilic cations. After incubation, a neutral red solution (100 µg/ml) was dissolved in serum-free culture medium for 2 h at 37°C and 5% CO_2, washed twice with PBS by centrifugation at 1,400 × *g* for 15 min. Next, 0.1 ml of extraction solution (ethanol/acetic acid, 50%/1%) was added to each well. The absorbance of the incorporated neutral red was measured at 540 nm using a microplate ELISA reader (Bio-Rad, Hercules, CA, USA).

Oxygen consumption assay. The rates of cell respiration were measured polarographically as described previously.[64, 68] The 0.6 ml reaction mixture contained the following: PBS, pH 7.4, 0.013 µg of digitonin per mg of cellular

protein (for permeabilizing plasma membrane), 10 mM succinate as the substrate and 2.5 mg of protein/ml of tumor cells supplemented with 1 µg/ml oligomycin. Respiration was initiated by adding the lipophilic cation derivatives of GA, which were added into 3 µl of DMSO using DMSO stocks prepared at different concentrations. At the end of the run, 0.15 µM FCCP (TA3 cell line) and 0.25 µM FCCP (TA3-MTX-R cell line) were added to fully uncouple respiration, as previously described.[39] Mitochondrial oxygen consumption was also measured polarographically. The 2.0 ml reaction medium consisted of the following components: 200 mM sucrose, 50 mM KCl, 3.0 mM potassium phosphate, 3.0 mM Hepes, pH 7.0, 2.0 mM $MgCl_2$ and 1.0 mg/ml of mitochondrial protein.[64, 68] Substrate concentrations were 2.0 mM glutamate plus 2.0 mM malate and 0.5 mM ADP. Other additions included 2.0 µg oligomycin and KCN 0.1 mM. The system was equilibrated with mitochondria at 25ºC for 2 min. Next, the rates of O_2 consumption were determined. All measurements were made as quickly as possible after the isolation of mitochondria.

Measurement of mitochondrial transmembrane potential changes. Changes in transmembrane potential ($\Delta\Psi_m$) were determined using the safranin method as previously described.[69] Changes of $\Delta A_{511\text{-}533}$ nm were assessed by spectrophotometry of the mitochondria. The reaction medium (2.5 ml) contained the following final concentrations: 200 mM sucrose, 50 mM KCl, 3 mM Hepes (pH 7.4), 0.5 mM EGTA, 3 mM potassium phosphate, 2 mM $MgCl_2$ and 1.0 mg/ml of mitochondrial protein. Mitochondria from the tumor cells were incubated with 20 µM safranin, and readings were collected for 5 min. Next, 2 mM glutamate and 2 mM

malate were added, and new readings were collected for 5 min. Finally, the cations were added, and the final readings were obtained.

Determination of mitochondrial transmembrane potential in whole cells using JC-1. A total of $1x10^6$ TA3/Ha cells/ml were seeded into 6-well plates. They were exposed to 10 μM TPP^+C_{10} or 10 μM CCCP (as a positive control). The cells were incubated for 1 h and then centrifuged at 1,500 × *g* for 5 min. The resulting precipitates were resuspended in 1 ml of PBS and then centrifuged at 1,500 × *g* for 5 min. The resulting precipitates were resuspended in 1 ml PBS at 37℃, and we added JC-1 (1 mg/ml in DMSO) and incubated the mixtures for 15 min at 37℃ in the dark. Next, the samples were centrifuged at 1,500 × *g* for 5 min, and the supernatants, which contained unincorporated JC-1, were discarded. The precipitates were suspended in PBS (3 ml) and measured for fluorescence using a JASCO FP-6200 spectrofluorometer. For the JC-1 monomers, the wavelengths used for excitation and emission were 485 and 540 nm, respectively, whereas those for the J-aggregates were 485 and 590 nm.

Mitochondrial swelling assay. To assess mitochondrial swelling, changes in side scatter of 540 ± 1 nm of a 0.5 mg/ml suspension of mitochondria in experimental buffer (125 mM KCl, 10 mM Tris-HCl [pH 7.4], 1 mM Pi, 5 mM glutamate, 2.5 mM malate, and 10 μM EGTA-Tris [pH 7.4]) were monitored using a JASCO V-560 UV/VIS Spectrophotometer.[70] The data are expressed as the difference in the absorbance prior to and after the addition of the stimulus. Each point corresponds to the mean values ± SEM of 3 independent experiments.

Intracellular NAD(P)H levels. NAD(P)H fluorescence (excitation and emission, 340 and 420 nm, respectively) was measured using a JASCO FP-6200

spectrofluorometer (JASCO Corporation Tokyo, Japan) equipped with magnetic stirring and thermostatic controls (25℃). The final reaction mixture (2.0 ml) contained the following components: PBS, pH 7.4, 2.5 mM glutamine as the substrate and 2.5 mg of protein/ml of the TA3 tumor cells.[71] Rotenone, FCCP or TPP^+C_{10} was added as indicated by arrows in the figures.

Intracellular levels of ATP. Intracellular ATP levels were measured using the CellTiter-Glo Luminescent Assay (Promega, USA) according to the manufacturer's protocols. Briefly, 2×10^5 cells/ml was incubated in a 24-well plate with the different cation GA derivatives for the indicated periods of time. Next, an aliquot of the cell suspension was transferred to an opaque 96-well plate, maintained at room temperature for 10 minutes in the dark and then measured for luminescence using a Thermo Scientific Varioskan® Flash spectral scanning multimode reader. Cell membrane integrity was assessed by PI incorporation as previously described.[72] This method was used as a control assay for cell viability for the measurement of intracellular ATP content. Briefly, 10^5 cells/well were placed in a 24-well plate and incubated with different concentrations of the compounds for the indicated times. Next, PI (10 µg/ml) was added to each well, and the cells were analyzed by flow cytometry (BD FACS Canto).

Western blotting. After the treatments, the cells were washed in PBS and then lysed with RIPA buffer (radioimmunoprecipitation assay) buffer, Tris-Cl 50 mM; NaCl 150 mM; sodium dodecyl sulfate (SDS) 0.1%; containing proteinase inhibitor cocktail and phosphatate inhibitor cocktail (Roche, Indianapolis, IN, USA). The lysate was centrifuged at 3000 × *g* at 4℃ for 10 min. The supernatants were collected, and the protein concentrations were determined using a BCA protein

assay kit (Pierce, Rockford, IL, USA). Fifty micrograms of proteins was separated by 12% SDS-polyacrylamide gel electrophoresis (SDS-PAGE), and the resolved proteins were transferred to a methylcellulose membrane (Millipore, Billerica, MA, USA). The membrane was blocked with 5% non-fat milk in Tris-buffered saline containing 0.1% Tween-20 (TBST) at room temperature for 1 h and then incubated with the primary antibodies at 4°C overnight. After washing with TBST, the membrane was incubated with anti-mouse or anti-rabbit horseradish peroxidase-conjugated secondary antibodies. Antibodies against caspases 3 (dilution 1:1,000) or tubulin (dilution 1:10,000) were incubated overnight at 4°C. The secondary antibodies (dilution 1:5,000) were incubated for 2 h at room temperature. After washing, the membranes were exposed to enhanced chemoluminescent (ECL) reagent. BioMax film was used for western blotting. The blots were quantified by laser scanning densitometry.

Apoptosis by flow cytometry. The apoptotic events induced by the cationic GA derivatives were determined by Annexin V staining and PI according to the manufacturer's protocol for the Annexin V-FITC Apoptosis Detection Kit (Abcam). For these analyses, we used 1 x 10^5 cells/ml, which were incubated at 37°C and 5% CO_2 with the various lipophilic cations for 24 and 48 h. The cells were resuspended in 500 µL of 1X Annexin V-binding buffer, and 5 µL each of Annexin V and PI were added to each sample (per the manufacturer's protocol). Next, we incubated the cells for 5 min at room temperature and then subjected them to flow cytometric analysis (FACS Canto, BD Biosciences, San Jose, CA, USA) at the following wavelengths: Annexin V FITC, Ex/Em = 488/530 nm, and PI, Ex/Em =

488/575 nm. For each sample, 5,000 events were recorded. The results were analyzed using the Cyflogic program (non-commercial version, CyFlo Ltd.). [73]

LDH activity. Lactate dehydrogenase release into the extracellular medium was evaluated using an LDH-Cytotoxicity Kit II (Abcam) according to the manufacturer's protocol. We used 2 x 10^5 cells/ml per assay. The cells were incubated in the presence or absence of the GA derivatives in an environment with 90% humidity, 5% CO_2 and 37℃ for the indicated times. Next, the plates were gently shaken to homogenize the LDH content. The cells were centrifuged at 600 × *g* for 3 min, and then 10-µl aliquots were transferred into each well of cell-free medium in a 96-well plate. Next, we added 100 µl of LDH reaction mix into each well, and the plate was incubated for 30 min at room temperature. The absorbance measurements were performed at 450 nm using a plate reader (BioRad, Hercules, CA, USA).

Evaluation of the antitumor activity of the alkyl triphenylphosphonium cation *in vivo*. Adult male CAF1-Jax mice were used. To determine tumor size, an external model was used. Briefly, 1.0 x 10^6 TA3/Ha cells/0.1 ml of 0.9% NaCl were injected subcutaneously into the backs of mice. Ten milligrams of TPP^+C_{10}/kg of body weight was administered i.p. to groups of 6 mice every 48 h for 30 days. During this period, we measured the minimum and maximum diameters (in millimeters) of tumors 3 times per week. The tumor volumes were calculated using the following formula: V = [(maximum diameter) x (minimum diameter)^2] / 2.[74] These volumes were compared with the control mouse group, which received a vehicle treatment. This protocol was duly approved by the bioethics committee of the Faculty of Medicine, University of Chile.

Statistical and regression analysis. The data were analyzed by two-way ANOVA with a Bonferroni post-test. The IC_{50} was calculated using a dose-response curve with a variable slope. GraphPad Prism was also used to find the best-fit linear regression (log-log plots), deduce the slopes and differences between slopes and determine the significance of the differences between the means by ANOVA. The differences were considered significant at $P < 0.05$.

Author contributions.

J.A.J., A.M. and J.F. designed the study, analyzed the data and wrote the manuscript. J.A.J., M.P., L.P. and F.J. performed most of the experimental work. V.C. and J.S. performed the organic synthesis. U.K., M.E.L., M.I.B., E.P. and J.M. contributed to project development and data interpretation.

Disclosure.

No financial disclosure.

Conflict of interest statement.

None.

List of abbreviations.

ANT: Adenine nucleotide translocase, **ATC**: Atractyloside, **CsA**: Cyclosporine A, **CPT**: Cisplatin, **CCCP**: Carbonyl cyanide *m*-chlorophenyl hydrazine, **FCCP**: Carbonyl cyanide *p*-trifluoromethoxyphenylhydrazone, **DNP**: 2,4-dinitrophenol, **DOX**: Doxorubicin, **DTT**: Dithiothreitol, **GA**: Gallic acid, **HK-II**: Hexokinase II, **IMM**: Inner mitochondrial membrane, **LG**: Lauryl Gallate, $\Delta\Psi_m$: Mitochondrial membrane potential, **MTX**: Methotrexate, **NAC**: N-acetylcysteine, **NEM**: N-ethylmaleimide, **OG**: Octyl Gallate, **Ph3P**: Triphenylphosphane, **TPP**: Triphenylphosphonium moiety.

Acknowledgement.

This work was supported by FONDECYT 1090075, 1130772, Anillo ACT-112 and a Ph.D. Fellowship to J.J. (CONICYT 21080199).

References

1. Fiuza, S. M.; Gomes, C.; Teixeira, L. J.; Girao da Cruz, M. T.; Cordeiro, M. N.; Milhazes, N.; Borges, F.; Marques, M. P. Phenolic acid derivatives with potential anticancer properties--a structure-activity relationship study. Part 1: methyl, propyl and octyl esters of caffeic and gallic acids. *Bioorg Med Chem* **2004,** *12*, 3581-3589.

2. Calcabrini, A.; Garcia-Martinez, J. M.; Gonzalez, L.; Tendero, M. J.; Ortuno, M. T.; Crateri, P.; Lopez-Rivas, A.; Arancia, G.; Gonzalez-Porque, P.; Martin-Perez, J. Inhibition of proliferation and induction of apoptosis in human breast cancer cells by lauryl gallate. *Carcinogenesis* **2006,** *27*, 1699-1712.

3. Fujita, K.; Kubo, I. Plasma membrane injury induced by nonyl gallate in Saccharomyces cerevisiae. *J Appl Microbiol* **2002,** *92*, 1035-1042.

4. Heijnen, C. G.; Haenen, G. R.; Vekemans, J. A.; Bast, A. Peroxynitrite scavenging of flavonoids: structure activity relationship. *Environ Toxicol Pharmacol* **2001,** *10*, 199-206.

5. Campos, A. M.; Ponce, E.; Lissi, E. A. Effects of alkyl chain lengths of gallates upon their distribution and reactivity towards diphenylpicryl hydracil radicals in Triton X-100 micellar solutions. *J Phys Org Chem* **2009,** *22*, 1208-1211.

6. Bridi, R.; Aliaga, C.; Aspee, A.; Abuin, E.; Lissi, E. Distribution and reactivity of gallates toward galvinoxyl radicals in SDS micellar solutions - Effect of the alkyl chain length. *Can J Chem* **2011,** *89*, 181-185.

7. Takai, E.; Hirano, A.; Shiraki, K. Effects of alkyl chain length of gallate on self-association and membrane binding. *J Biochem* **2011,** *150*, 165-171.

8. Campos, A.; Villalobos, C.; Lissi, E. Reaction of Alkyl Gallates with Diphenyl Picrylhydracyl Radicals in Sds Micelles. *J Chil Chem Soc* **2010,** *55*, 458-460.

9. Madlener, S.; Saiko, P.; Vonach, C.; Viola, K.; Huttary, N.; Stark, N.; Popescu, R.; Gridling, M.; Vo, N. T.; Herbacek, I.; Davidovits, A.; Giessrigl, B.; Venkateswarlu, S.; Geleff, S.; Jager, W.; Grusch, M.; Kerjaschki, D.; Mikulits, W.; Golakoti, T.; Fritzer-Szekeres, M.; Szekeres, T.; Krupitza, G. Multifactorial anticancer effects of digalloyl-resveratrol encompass apoptosis, cell-cycle arrest, and inhibition of lymphendothelial gap formation in vitro. *Br J Cancer* **2010,** *102*, 1361-1370.

10. Bernhaus, A.; Fritzer-Szekeres, M.; Grusch, M.; Saiko, P.; Krupitza, G.; Venkateswarlu, S.; Trimurtulu, G.; Jaeger, W.; Szekeres, T. Digalloylresveratrol, a new phenolic acid derivative induces apoptosis and cell cycle arrest in human HT-29 colon cancer cells. *Cancer Lett* **2009,** *274*, 299-304.

11. Rosso, R.; Vieira, T. O.; Leal, P. C.; Nunes, R. J.; Yunes, R. A.; Creczynski-Pasa, T. B. Relationship between the lipophilicity of gallic acid n-alquil esters'

derivatives and both myeloperoxidase activity and HOCl scavenging. *Bioorg Med Chem* **2006,** *14*, 6409-6413.

12. Uozaki, M.; Yamasaki, H.; Katsuyama, Y.; Higuchi, M.; Higuti, T.; Koyama, A. H. Antiviral effect of octyl gallate against DNA and RNA viruses. *Antiviral Res* **2007,** *73*, 85-91.

13. Hurtado, C.; Bustos, M. J.; Sabina, P.; Nogal, M. L.; Granja, A. G.; Gonzalez, M. E.; Gonzalez-Porque, P.; Revilla, Y.; Carrascosa, A. L. Antiviral activity of lauryl gallate against animal viruses. *Antivir Ther* **2008,** *13*, 909-917.

14. Kratz, J. M.; Andrighetti-Frohner, C. R.; Kolling, D. J.; Leal, P. C.; Cirne-Santos, C. C.; Yunes, R. A.; Nunes, R. J.; Trybala, E.; Bergstrom, T.; Frugulhetti, I. C.; Barardi, C. R.; Simoes, C. M. Anti-HSV-1 and anti-HIV-1 activity of gallic acid and pentyl gallate. *Mem Inst Oswaldo Cruz* **2008,** *103*, 437-442.

15. Shibata, H.; Nakano, T.; Parvez, M. A.; Furukawa, Y.; Tomoishi, A.; Niimi, S.; Arakaki, N.; Higuti, T. Triple combinations of lower and longer alkyl gallates and oxacillin improve antibiotic synergy against methicillin-resistant Staphylococcus aureus. *Antimicrob Agents Chemother* **2009,** *53*, 2218-2220.

16. Shibata, H.; Kondo, K.; Katsuyama, R.; Kawazoe, K.; Sato, Y.; Murakami, K.; Takaishi, Y.; Arakaki, N.; Higuti, T. Alkyl gallates, intensifiers of beta-lactam susceptibility in methicillin-resistant Staphylococcus aureus. *Antimicrob Agents Chemother* **2005,** *49*, 549-555.

17. Stapleton, P. D.; Shah, S.; Anderson, J. C.; Hara, Y.; Hamilton-Miller, J. M.; Taylor, P. W. Modulation of beta-lactam resistance in Staphylococcus aureus by catechins and gallates. *Int J Antimicrob Agents* **2004,** *23*, 462-467.

18. Leal, P. C.; Mascarello, A.; Derita, M.; Zuljan, F.; Nunes, R. J.; Zacchino, S.; Yunes, R. A. Relation between lipophilicity of alkyl gallates and antifungal activity against yeasts and filamentous fungi. *Bioorg Med Chem Lett* **2009,** *19*, 1793-1796.

19. Hsu, F. L.; Chen, P. S.; Chang, H. T.; Chang, S. T. Effects of alkyl chain length of gallates on their antifungal property and potency as an environmentally benign preservative against wood-decay fungi. *Int Biodeterior Biodegrad* **2009,** *36*, 543-547.

20. Kim, J. H.; Campbell, B. C.; Mahoney, N.; Chan, K. L.; Molyneux, R. J.; Xiao, C. L. Use of chemosensitization to overcome fludioxonil resistance in Penicillium expansum. *Let Appl Microbiol* **2010,** *51*, 177-183.

21. Yeh, R. D.; Chen, J. C.; Lai, T. Y.; Yang, J. S.; Yu, C. S.; Chiang, J. H.; Lu, C. C.; Yang, S. T.; Yu, C. C.; Chang, S. J.; Lin, H. Y.; Chung, J. G. Gallic acid induces G(0)/G(1) phase arrest and apoptosis in human leukemia HL-60 cells through inhibiting cyclin D and E, and activating mitochondria-dependent pathway. *Anticancer Res* **2011,** *31*, 2821-2832.

22. Frey, C.; Pavani, M.; Cordano, G.; Munoz, S.; Rivera, E.; Medina, J.; Morello, A.; Maya, J. D.; Ferreira, J. Comparative cytotoxicity of alkyl gallates on

mouse tumor cell lines and isolated rat hepatocytes. *Comp Biochem Physiol A:Mol Integr Physiol* **2007,** *146*, 520-527.

23. de Cordova, C. A. S.; Locatelli, C.; Assuncao, L. S.; Mattei, B.; Mascarello, A.; Winter, E.; Nunes, R. J.; Yunes, R. A.; Creczynski-Pasa, T. B. Octyl and dodecyl gallates induce oxidative stress and apoptosis in a melanoma cell line. *Toxicol in Vitro* **2011,** *25*, 2025-2034.

24. Locatelli, C.; Leal, P. C.; Yunes, R. A.; Nunes, R. J.; Creczynski-Pasa, T. B. Gallic acid ester derivatives induce apoptosis and cell adhesion inhibition in melanoma cells: The relationship between free radical generation, glutathione depletion and cell death. *Chem Biol Interact* **2009,** *181*, 175-184.

25. Lopez-Rios, F.; Sanchez-Arago, M.; Garcia-Garcia, E.; Ortega, A. D.; Berrendero, J. R.; Pozo-Rodriguez, F.; Lopez-Encuentra, A.; Ballestin, C.; Cuezva, J. M. Loss of the mitochondrial bioenergetic capacity underlies the glucose avidity of carcinomas. *Cancer Res* **2007,** *67*, 9013-9017.

26. Putignani, L.; Raffa, S.; Pescosolido, R.; Aimati, L.; Signore, F.; Torrisi, M. R.; Grammatico, P. Alteration of expression levels of the oxidative phosphorylation system (OXPHOS) in breast cancer cell mitochondria. *Breast Cancer Res Treat* **2008,** *110*, 439-452.

27. Modica-Napolitano, J. S.; Singh, K. K. Mitochondrial dysfunction in cancer. *Mitochondrion* **2004,** *4*, 755-762.

28. Gourley, P. L.; Hendricks, J. K.; McDonald, A. E.; Copeland, R. G.; Barrett, K. E.; Gourley, C. R.; Singh, K. K.; Naviaux, R. K. Mitochondrial correlation microscopy and nanolaser spectroscopy - New tools for biophotonic detection of cancer in single cells. *Tech Canc Res Treat* **2005,** *4*, 585-592.

29. Rossignol, R.; Gilkerson, R.; Aggeler, R.; Yamagata, K.; Remington, S. J.; Capaldi, R. A. Energy substrate modulates mitochondrial structure and oxidative capacity in cancer cells. *Cancer Res* **2004,** *64*, 985-993.

30. Christofk, H. R.; Vander Heiden, M. G.; Harris, M. H.; Ramanathan, A.; Gerszten, R. E.; Wei, R.; Fleming, M. D.; Schreiber, S. L.; Cantley, L. C. The M2 splice isoform of pyruvate kinase is important for cancer metabolism and tumour growth. *Nature* **2008,** *452*, 230-233.

31. Rodriguez-Enriquez, S.; Marin-Hernandez, A.; Gallardo-Perez, J. C.; Carreno-Fuentes, L.; Moreno-Sanchez, R. Targeting of cancer energy metabolism. *Mol Nutr Food Res* **2009,** *53*, 29-48.

32. Pedersen, P. L. The cancer cell's "power plants" as promising therapeutic targets: An overview. *J Bioenerg Biomembr* **2007,** *39*, 1-12.

33. Rosano, C. Molecular model of hexokinase binding to the outer mitochondrial membrane porin (VDAC1): Implication for the design of new cancer therapies. *Mitochondrion* **2011,** *11*, 513-519.

34. Modica-Napolitano, J. S.; Singh, K. K. Mitochondrial dysfunction in cancer. *Mitochondrion* **2004,** *4*, 755-762.

35. Coulter, C. V.; Kelso, G. F.; Lin, T. K.; Smith, R. A.; Murphy, M. P. Mitochondrially targeted antioxidants and thiol reagents. *Free Radic Biol Med* **2000,** *28*, 1547-1554.

36. Ross, M. F.; Kelso, G. F.; Blaikie, F. H.; James, A. M.; Cocheme, H. M.; Filipovska, A.; Da Ros, T.; Hurd, T. R.; Smith, R. A. J.; Murphy, M. P. Lipophilic triphenylphosphonium cations as tools in mitochondrial bioenergetics and free radical biology. *Biochemistry-Moscow* **2005,** *70*, 222-230.

37. Murphy, M. P.; Smith, R. A. Targeting antioxidants to mitochondria by conjugation to lipophilic cations. *Annu Rev Pharmacol Toxicol* **2007,** *47*, 629-656.

38. Moreno-Sanchez, R.; Rodriguez-Enriquez, S.; Marin-Hernandez, A.; Saavedra, E. Energy metabolism in tumor cells. *FEBS J* **2007,** *274*, 1393-1418.

39. Lou, P. H.; Hansen, B. S.; Olsen, P. H.; Tullin, S.; Murphy, M. P.; Brand, M. D. Mitochondrial uncouplers with an extraordinary dynamic range. *Biochem J* **2007,** *407*, 129-140.

40. Jana, F.; Faini, F.; Lapier, M.; Pavani, M.; Kemmerling, U.; Morello, A.; Maya, J. D.; Jara, J.; Parra, E.; Ferreira, J. Tumor cell death induced by the inhibition of mitochondrial electron transport: The effect of 3-hydroxybakuchiol. *Toxicol Appl Pharmacol* **2013,** 272, 356-364.

41. Zhang, L.; Yang, N.; Garcia, J. R.; Mohamed, A.; Benencia, F.; Rubin, S. C.; Allman, D.; Coukos, G. Generation of a syngeneic mouse model to study the effects of vascular endothelial growth factor in ovarian carcinoma. *Am J Pathol* **2002,** *161*, 2295-2309.

42. Ebos, J. M.; Lee, C. R.; Cruz-Munoz, W.; Bjarnason, G. A.; Christensen, J. G.; Kerbel, R. S. Accelerated metastasis after short-term treatment with a potent inhibitor of tumor angiogenesis. *Cancer Cell* **2009,** *15*, 232-239.

43. Rodriguez-Enriquez, S.; Marin-Hernandez, A.; Gallardo-Perez, J. C.; Carreno-Fuentes, L.; Moreno-Sanchez, R. Targeting of cancer energy metabolism. *Mol Nutr Food Res* **2009,** *53*, 29-48.

44. Pathania, D.; Millard, M.; Neamati, N. Opportunities in discovery and delivery of anticancer drugs targeting mitochondria and cancer cell metabolism. *Adv Drug Deliv Rev* **2009,** *61*, 1250-1275.

45. You, B. R.; Park, W. H. Gallic acid-induced lung cancer cell death is related to glutathione depletion as well as reactive oxygen species increase. *Toxicol In Vitro* **2010,** *24*, 1356-1362.

46. Punithavathi, V. R.; Prince, P. S. M.; Kumar, R.; Selvakumari, J. Antihyperglycaemic, antilipid peroxidative and antioxidant effects of gallic acid on streptozotocin induced diabetic Wistar rats. *Eur J Pharmacol* **2011,** 650, 465-471.

47. Mayevsky, A.; Rogatsky, G. G. Mitochondrial function in vivo evaluated by NADH fluorescence: from animal models to human studies. *Am J Physiol Cell Physiol* **2007,** *292*, C615-C640.

48. Murphy, M. P. Mitochondrial Thiols in Antioxidant Protection and Redox Signaling: Distinct Roles for Glutathionylation and Other Thiol Modifications. *Antioxid Redox Signal* **2012,** *16*, 476-495.

49. Rodriguez-Enriquez, S.; Gallardo-Perez, J. C.; Marin-Hernandez, A.; Moreno-Sanchez, R. The Warburg Hypothesis and the ATP Supply In Cancer Cells Is Oxidative Phosphorylation impaired in malignant neoplasias? *Curr Pharm Biotechnol* **2012,** *Jun. 1.*

50. Han, Y. H.; Moon, H. J.; You, B. R.; Kim, S. Z.; Kim, S. H.; Park, W. H. Effects of carbonyl cyanide p-(trifluoromethoxy) phenylhydrazone on the growth inhibition in human pulmonary adenocarcinoma Calu-6 cells. *Toxicology* **2009,** *265*, 101-107.

51. Nadtochiy, S. M.; Tompkins, A. J.; Brookes, P. S. Different mechanisms of mitochondrial proton leak in ischaemia/reperfusion injury and preconditioning: implications for pathology and cardioprotection. *Biochem J* **2006,** *395*, 611-618.

52. Battaglia, V.; Salvi, M.; Toninello, A. Oxidative stress is responsible for mitochondrial permeability transition induction by salicylate in liver mitochondria. *J Biol Chem* **2005,** *280*, 33864-33872.

53. Brustovetsky, T.; Li, T.; Yang, Y.; Zhang, J. T.; Antonsson, B.; Brustovetsky, N. BAX insertion, oligomerization, and outer membrane permeabilization in brain mitochondria: role of permeability transition and SH-redox regulation. *Biochim Biophys Acta* **2010,** *1797*, 1795-806.

54. Kilbride, S. M.; Prehn, J. H. Central roles of apoptotic proteins in mitochondrial function. *Oncogene* **2012,** *32*, 2703-2711.

55. Basanez, G.; Soane, L.; Hardwick, J. M. A new view of the lethal apoptotic pore. *PLoS Biol* **2012,** *10*, e1001399.

56. Ng, H.; Smith, D. J.; Nagley, P. Application of flow cytometry to determine differential redistribution of cytochrome c and Smac/DIABLO from mitochondria during cell death signaling. *Plos One* **2012,** *7*, e42298.

57. Takeda, M.; Kobayashi, M.; Shirato, I.; Osaki, T.; Endou, H. Cisplatin-induced apoptosis of immortalized mouse proximal tubule cells is mediated by interleukin-1 beta converting enzyme (ICE) family of proteases but inhibited by overexpression of Bcl-2. *Arch Toxicol* **1997,** *71*, 612-621.

58. Locatelli, C.; Carvalho, D. R.; Mascarello, A.; de Cordova, C. A.; Yunes, R. A.; Nunes, R. J.; Pilati, C.; Creczynski-Pasa, T. B. Antimetastatic activity and low

systemic toxicity of tetradecyl gallate in a preclinical melanoma mouse model. *Invest New Drugs* **2012,** *30*, 870-879.

59. Prime, T. A.; Blaikie, F. H.; Evans, C.; Nadtochiy, S. M.; James, A. M.; Dahm, C. C.; Vitturi, D. A.; Patel, R. P.; Hiley, C. R.; Abakumova, I.; Requejo, R.; Chouchani, E. T.; Hurd, T. R.; Garvey, J. F.; Taylor, C. T.; Brookes, P. S.; Smith, R. A.; Murphy, M. P. A mitochondria-targeted S-nitrosothiol modulates respiration, nitrosates thiols, and protects against ischemia-reperfusion injury. *Proc Natl Acad Sci USA* **2009,** *106*, 10764-10769.

60. Kelso, G. F.; Porteous, C. M.; Coulter, C. V.; Hughes, G.; Porteous, W. K.; Ledgerwood, E. C.; Smith, R. A.; Murphy, M. P. Selective targeting of a redox-active ubiquinone to mitochondria within cells: antioxidant and antiapoptotic properties. *J Biol Chem* **2001,** *276*, 4588-4596.

61. Covey, M. V.; Murphy, M. P.; Hobbs, C. E.; Smith, R. A.; Oorschot, D. E. Effect of the mitochondrial antioxidant, Mito Vitamin E, on hypoxic-ischemic striatal injury in neonatal rats: a dose-response and stereological study. *Exp Neurol* **2006,** *199*, 513-519.

62. Brown, S. E.; Ross, M. F.; Sanjuan-Pla, A.; Manas, A. R.; Smith, R. A.; Murphy, M. P. Targeting lipoic acid to mitochondria: synthesis and characterization of a triphenylphosphonium-conjugated alpha-lipoyl derivative. *Free Radic Biol Med* **2007,** *42*, 1766-1780.

63. Fones, E.; Amigo, H.; Gallegos, K.; Guerrero, A.; Ferreira, J. t-butyl-4-hydroxyanisole as an Inhibitor of Tumor-Cell Respiration. *Biocheml Pharmacol* **1989,** *38*, 3443-3451.

64. Plaza, C.; Pavani, M.; Faundez, M.; Maya, J. D.; Morello, A.; Becker, M. I.; De Ioannes, A.; Cumsille, M. A.; Ferreira, J. Inhibitory effect of nordihydroguaiaretic acid and its tetra-acetylated derivative on respiration and growth of adenocarcinoma TA3 and its multiresistant variant TA3MTX-R. *In Vivo* **2008,** *22*, 353-361.

65. Moreadith, R. W.; Fiskum, G. Isolation of mitochondria from ascites tumor cells permeabilized with digitonin. *Anal Biochem* **1984,** *137*, 360-367.

66. Lowry, O. H.; Rosebrough, N. J.; Farr, A. L.; Randall, R. J. Protein measurement with the Folin phenol reagent. *J Biol Chem* **1951,** *3*, 1125-1131.

67. Repetto, G.; del Peso, A.; Zurita, J. L. Neutral red uptake assay for the estimation of cell viability/cytotoxicity. *Nature Protocols* **2008,** *3*, 1125-1131.

68. Proceedings of an international conference on anticancer drugs: therapeutic index improvement by toxicity reduction. London, 6-7 April 1987. *Cancer Treat Rev* **1987,** *14*, 157-420.

69. Pulselli, R.; Arcuri, E.; Paggi, M. G.; Floridi, A. Changes in membrane potential induced by local anesthetic bupivacaine on mitochondria within Ehrlich ascites tumor cells. *Oncol Res* **1996,** *8*, 267-271.

70. Fantin, V. R.; Berardi, M. J.; Scorrano, L.; Korsmeyer, S. J.; Leder, P. A novel mitochondriotoxic small molecule that selectively inhibits tumor cell growth. *Cancer Cell* **2002,** *2*, 29-42.

71. Eng, J.; Lynch, R. M.; Balaban, R. S. Nicotinamide adenine dinucleotide fluorescence spectroscopy and imaging of isolated cardiac myocytes. *Biophys J* **1989,** *55*, 621-630.

72. Moisenovich, M. M.; Ol'shevskaya, V. A.; Rokitskaya, T. I.; Ramonova, A. A.; Nikitina, R. G.; Savchenko, A. N.; Tatarskiy, V. V., Jr.; Kaplan, M. A.; Kalinin, V. N.; Kotova, E. A.; Uvarov, O. V.; Agapov, II; Antonenko, Y. N.; Shtil, A. A. Novel photosensitizers trigger rapid death of malignant human cells and rodent tumor transplants via lipid photodamage and membrane permeabilization. *PLoS One* **2010,** *5*, e12717.

73. Puig, T.; Vazquez-Martin, A.; Relat, J.; Petriz, J.; Menendez, J. A.; Porta, R.; Casals, G.; Marrero, P. F.; Haro, D.; Brunet, J.; Colomer, R. Fatty acid metabolism in breast cancer cells: differential inhibitory effects of epigallocatechin gallate (EGCG) and C75. *Breast Cancer Res Treat* **2008,** *109*, 471-479.

74. Jensen, M. M.; Jorgensen, J. T.; Binderup, T.; Kjaer, A. Tumor volume in subcutaneous mouse xenografts measured by microCT is more accurate and reproducible than determined by 18F-FDG-microPET or external caliper. *BMC Med Imaging* **2008,** *8*: 16.

Figure legends.

Figure 1. The delocalized lipophilic cations of gallic acid derivatives and their cytotoxic effects. A) Synthesis schedule of lipophilic cations of gallic acid derivatives. B) TA3 anti-proliferative effect. C) TA3/Ha sigmoidal dose-response curves (variable slope) showing the cytotoxic effect at 48 h of TPP^+C_{10} exposure. D) TA3-MTX-R sigmoidal dose-response curves showing the cytotoxic effect at 48 h of TPP^+C_{10} exposure. The results were obtained using the neutral red assay. The values represent the mean values of at least 3 independent experiments ± SEM. Each assay was performed in triplicate.

Figure 2. A) Representative traces of the effect of ADP, oligomycin, CN^- and TPP^+C_8 on the O_2 consumption in mitochondria from the TA3/Ha cell line in the presence of glutamate plus malate as substrates. B) Representative traces of the effects of TPP^+C_8 on the time course of O_2 consumption by the TA3/Ha mitochondria (oxidation of glutamate and malate). C) The uncoupling effect on intact cancer cells by the cationic GA derivatives. A double logarithmic plot of the uncoupling effects of the different GA derivatives on respiration in the TA3 and TA3-MTX-R cell lines. Closed circles (●) represent the titration of respiration rates induced by each GA derivative. The closed inverted triangles (▼) represent the titration of the respiration rates with each GA derivative in the presence of 5 nmol ATC/mg of protein (added before succinate). The open circles (○) represent the respiration rate at each concentration of each GA derivative after the addition of FCCP to attain the maximal cellular respiratory capacity. The values shown are the mean values ± SEM of at least 3 independent experiments. The lines were fitted by linear regression obtain from GraphPad Prism (4.0) plot software. Then, slope in

log-log plot and $K_{0.5}$ (M) values were calculated from linear regression equation. This latter value corresponds to the 50% of the maximal cellular respiratory capacity.

Figure 3. The lipophilic cation effect on intracellular ATP content. A-D) A total of 2 × 10^5 cells/ml were incubated for 2 h with each cation, and the ATP content was measured as described in the methods section. A) The effects of TPP^+C_8 on ATP levels. B) The effects of TPP^+C_{10} on ATP levels. C) The effects of TPP^+C_{11} on ATP levels. D) The effects of TPP^+C_{12} on ATP levels. E) The effects of increasing concentrations of lipophilic cations on cellular viability. The control test of cellular membrane integrity was measured by PI incorporation using a flow cytometer. A total of 2 × 10^5 cells/ml were seeded and incubated for 24 h at 37°C and 5% CO_2. Next, the culture medium was changed, the cationic GA derivatives were added, and the cells were incubated for 2 and 4 h. Propidium iodide (1 mg/ml) was then added. The values shown are the mean values ± SEM of at least 3 independent experiments. The error bars correspond to the confidence interval of 95%. * P <0.05 compared to the control group (ANOVA) followed by Bonferroni pos-test. * P < 0.05, ** P < 0.005, *** P < 0.001.

Figure 4. A) The effects of TPP^+C_{10} on NAD(P)H oxidation on the TA3/Ha cell line. Time course plots of NAD(P)H oxidation induced by TPP^+C_{10} (2.5 mg protein/ml) in the TA3/Ha cell line. We used 12 µM rotenone and 6 µM FCCP. B) The effect of ADP on the transmembrane potential ($\Delta\Psi_m$) of the mitochondria of TA3/Ha cells. C) The effects of TPP^+C_{10} on the $\Delta\Psi_m$ of the TA3-MTX-R cells. D) The effects of CCCP on the $\Delta\Psi_m$ of the TA3/Ha cells. The experiments were performed using 1

mg/ml of mitochondrial protein, 20 μM safranin, 250 μM ADP, 5 mM malate and either 5 mM glutamate or 0.2 nmol CCCP. The measurements were collected for 16.7 min. The values represent the average of at least 3 independent experiments ± SD. E) The effects of TPP^+C_{10} on the $\Delta\Psi_m$ of TA3/Ha cells measured using JC-1 fluorescent probe in presence of 3 μM FCCP and 0.5 μM TPP^+C_{10}. The values shown are the mean values ± SEM of at least 3 independent experiments. values shown are the mean values ± SEM of at least 3 independent experiments. The error bars correspond to the confidence interval of 95%. * P <0.05 compared to the control group (ANOVA) and followed by corresponding post test (Bonferroni).*** P < 0.001.

Figure 5. The effects of lipophilic cations on mitochondrial swelling. A) The effects of increasing concentrations of TPP^+C_{10} on the mitochondria of TA3/Ha (black bars) and TA3-MTX-R (solid bars). B) The effects of increasing concentrations of cyclosporine on the mitochondria of TA3/Ha cells in the presence of 0.15 mM TPP^+C_{10}. C) N-ethylmaleimide (NEM), D) dithiothreitol (DTT) and E) N-acetylcysteine (NAC) prevent the effect of 0.15 mM TPP^+C_{10} on the mitochondria of TA3/Ha cells. The values shown are the mean values ± SEM of at least 3 independent experiments. The error bars correspond to the confidence interval of 95%. * P <0.05 compared to the control group (ANOVA) and followed by corresponding post-test (Bonferroni). * P < 0.05, ** P < 0.005, *** P < 0.001.

Figure 6. The type of cell death. A) Western blot measurement of caspase 3 activation on the TA3/Ha cells in the presence of each compound at 0.5 μM for 24 h. The assay was conducted under the conditions listed in the methods section. B)

Cell cycle analysis of TA3/Ha cells after 24 h of treatment with increasing concentrations of TPP^+C_{10}. C) Representative dot-plots of PI and Annexin V double staining on the TA3/Ha cells in the presence of 0.5 µM of each cation or 10 µM staurosporine (SP) as a positive control for 24 h or D) 48 h of treatment. E) Quantifications of C and D, respectively. The values shown are the mean values ± SEM of at least 3 independent experiments. The error bars correspond to the confidence interval of 95%. * P <0.05 compared to the control group (ANOVA) followed by Bonferroni post-test.* $P < 0.05$, ** $P < 0.005$, *** $P < 0.001$.

Figure 7. The effect of TPP^+C_{10} on tumor growth in CAF1-Jax mice. A) Syngenic model: mice were administered 10 mg of TPP^+C_{10}/kg or vehicle via i.p. every 48 h for 30 days. The tumor sizes were measured externally 3 times per week. The graph shows the average tumor volumes (mm^3) from 2 independent experiments (n = 6 mice per group). B) Representative images of the tumor volumes. The error bars correspond to the confidence interval of 95%. * P <0.05 compared to the control group (nonparametric Mann-Whitney test followed by Wilcoxon post-test).

Table 1. Cytotoxicity of GA ester derivatives in the tumor cell lines TA3/Ha, TA3-MTX-R and CCRF-CEM and the non-tumoral cell line MM3MG.

	TA3/Ha	TA3-MTX-R	CCRF-CEM	MM3MG
Compound	IC_{50} µM			
GA	163.1 ± 2.3	160.2 ± 1.3	>200	>200
OG	35.9 ± 0.6	29.8 ± 0.3	58,5 ± 1,4	>200
LG	7.06 ± 0.1	3.00 ± 0.03	15,46 ± 0,1	30 ± 7
TPP^+C_8	13.4 ± 0.01	14.4 ± 0.01	34.6 ± 0.02	29.4 ± 8.7
TPP^+C_{10}	0.40 ± 0.01	0.38 ± 0.02	1.65 ± 0.2	7.1 ± 3.2
TPP^+C_{11}	6.4 ± 1.0	3.7 ± 0.8	19.75 ± 0.01	14.3 ± 2.5
TPP^+C_{12}	0.74 ± 0.09	1.2 ± 0.3	0.58 ± 0.21	1.38 ± 0.4
Ph3P	190 ± 2.5	>200	184± 5	>200

IC_{50} = the concentration resulting in cytotoxicity in 50% of cultured cells after 48 h of treatment. Values were calculated from the respective sigmoidal dose-response curves, representing the mean ± SEM values of at least 3 independent experiments. Each assay was performed in triplicate.

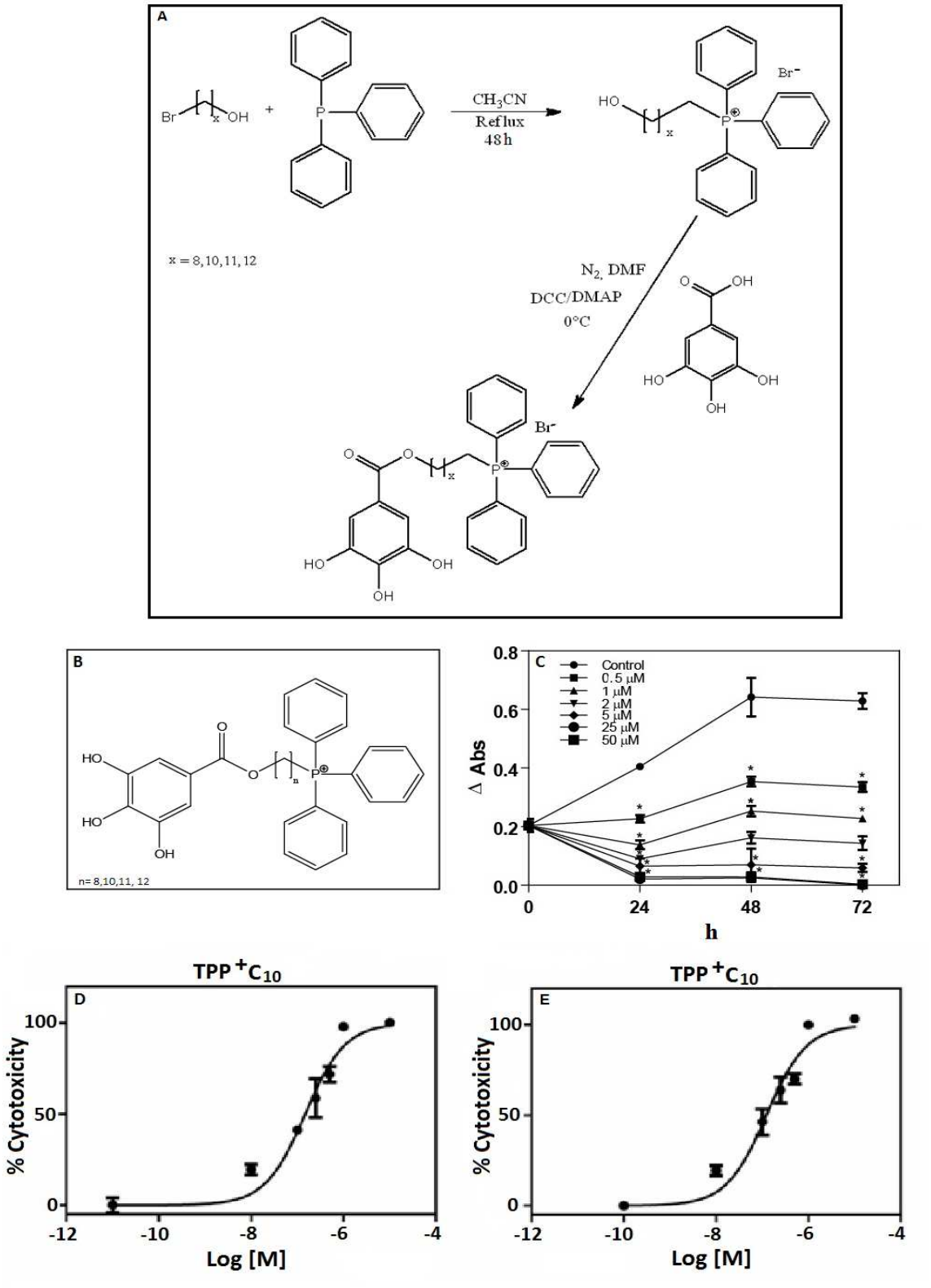
A
Br
OH
x
+
P
CH3CN
Reflux
48 h
HO
Br-
x = 8,10,11,12
N2, DMF
DCC/DMAP
0°C
O
OH
HO
OH
OH
B
HO
HO
OH
O
n
P
n= 8,10,11, 12
C
Control
0.5 μM
1 μM
2 μM
5 μM
25 μM
50 μM
Δ Abs
0.8
0.6
0.4
0.2
0.0
0
24
48
72
h
TPP+C10
D
% Cytotoxicity
100
50
0
-12
-10
-8
-6
-4
Log [M]
TPP+C10
E
% Cytotoxicity
100
50
0
-12
-10
-8
-6
-4
Log [M]

Figure 1

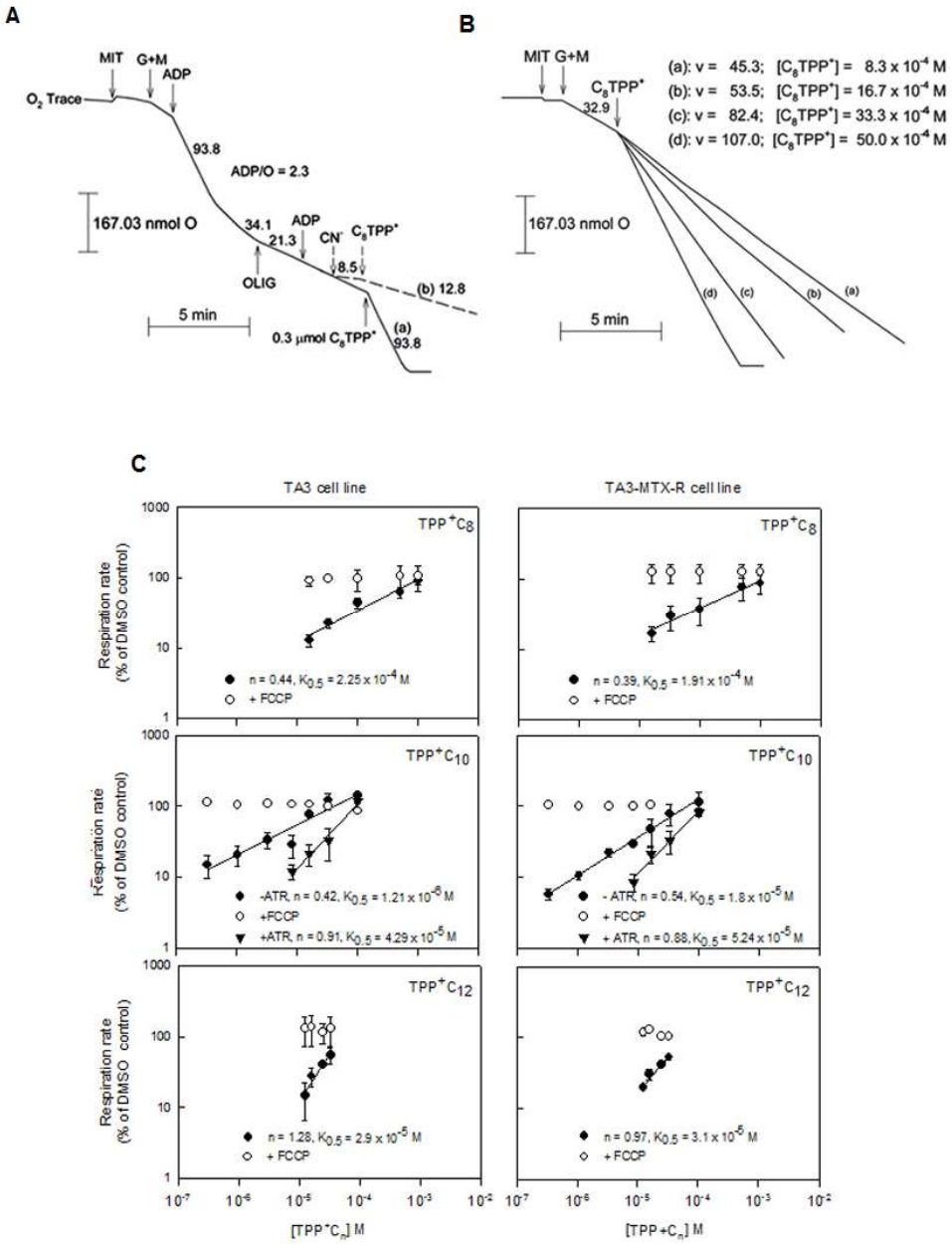
A
MIT G+M ADP
O2 Trace
93.8
ADP/O = 2.3
167.03 nmol O
34.1
21.3
ADP
CN-
C8TPP+
8.5
OLIG
(b) 12.8
5 min
0.3 µmol C8TPP+
(a) 93.8
B
MIT G+M
C8TPP+
32.9
(a): v = 45.3; [C8TPP+] = 8.3 x 10-4 M
(b): v = 53.5; [C8TPP+] = 16.7 x 10-4 M
(c): v = 82.4; [C8TPP+] = 33.3 x 10-4 M
(d): v = 107.0; [C8TPP+] = 50.0 x 10-4 M
167.03 nmol O
5 min
(d) (c) (b) (a)
C
TA3 cell line
TA3-MTX-R cell line
TPP+C8
TPP+C10
TPP+C12
Respiration rate (% of DMSO control)
n = 0.44, K0.5 = 2.25 x 10-4 M
+ FCCP
n = 0.39, K0.5 = 1.91 x 10-4 M
-ATR, n = 0.42, K0.5 = 1.21 x 10-6 M
+FCCP
+ATR, n = 0.91, K0.5 = 4.29 x 10-5 M
- ATR, n = 0.54, K0.5 = 1.8 x 10-5 M
+ ATR, n = 0.88, K0.5 = 5.24 x 10-5 M
n = 1.28, K0.5 = 2.9 x 10-5 M
n = 0.97, K0.5 = 3.1 x 10-5 M
[TPP+Cn] M

Figure 2

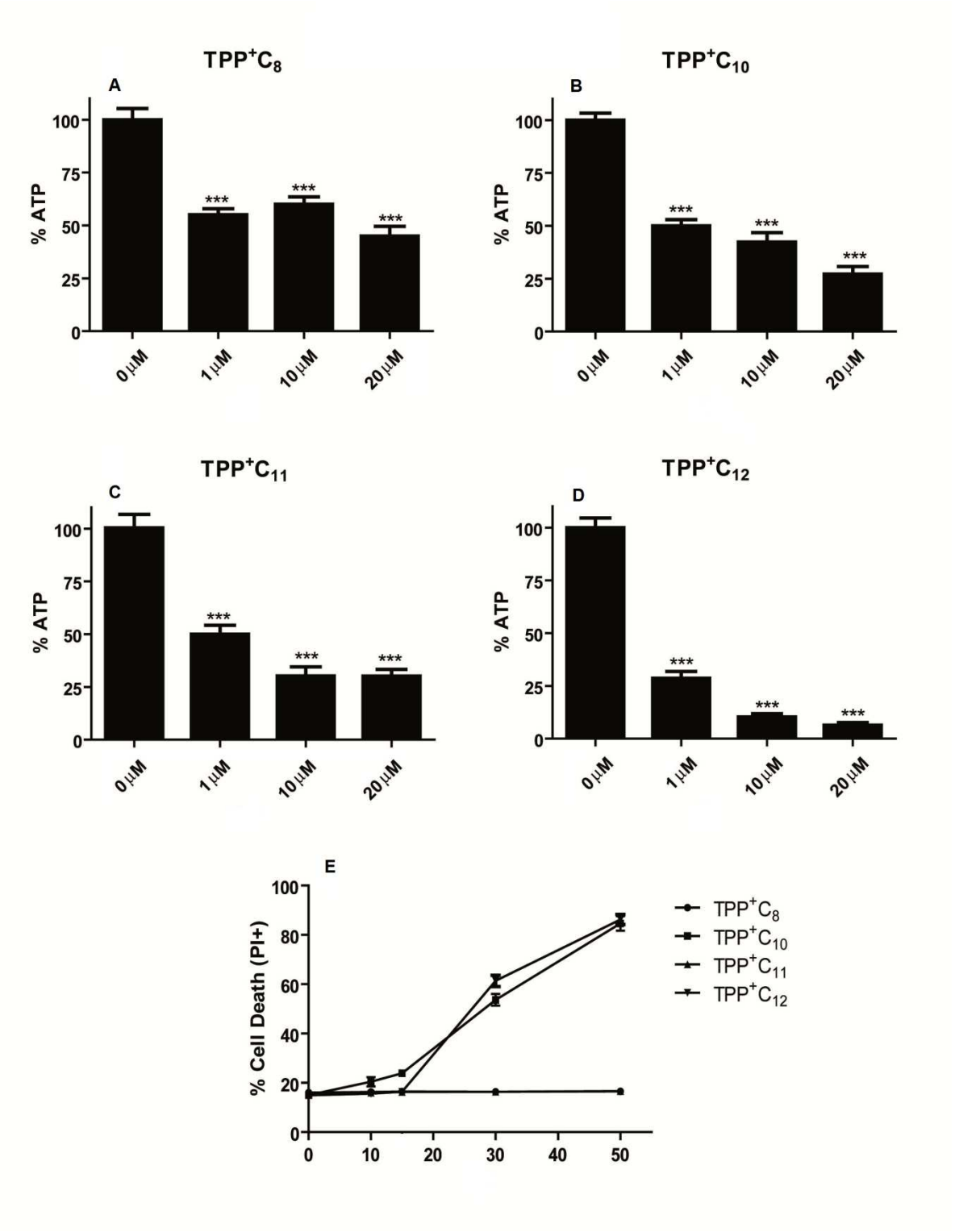
TPP+C8
A
% ATP
100
75
50
25
0
***
***
***
0 μM
1 μM
10 μM
20 μM
TPP+C10
B
% ATP
100
75
50
25
0
***
***
***
0 μM
1 μM
10 μM
20 μM
TPP+C11
C
% ATP
100
75
50
25
0
***
***
***
0 μM
1 μM
10 μM
20 μM
TPP+C12
D
% ATP
100
75
50
25
0
***
***
***
0 μM
1 μM
10 μM
20 μM
E
% Cell Death (PI+)
100
80
60
40
20
0
0
10
20
30
40
50
TPP+C8
TPP+C10
TPP+C11
TPP+C12

Figure 3

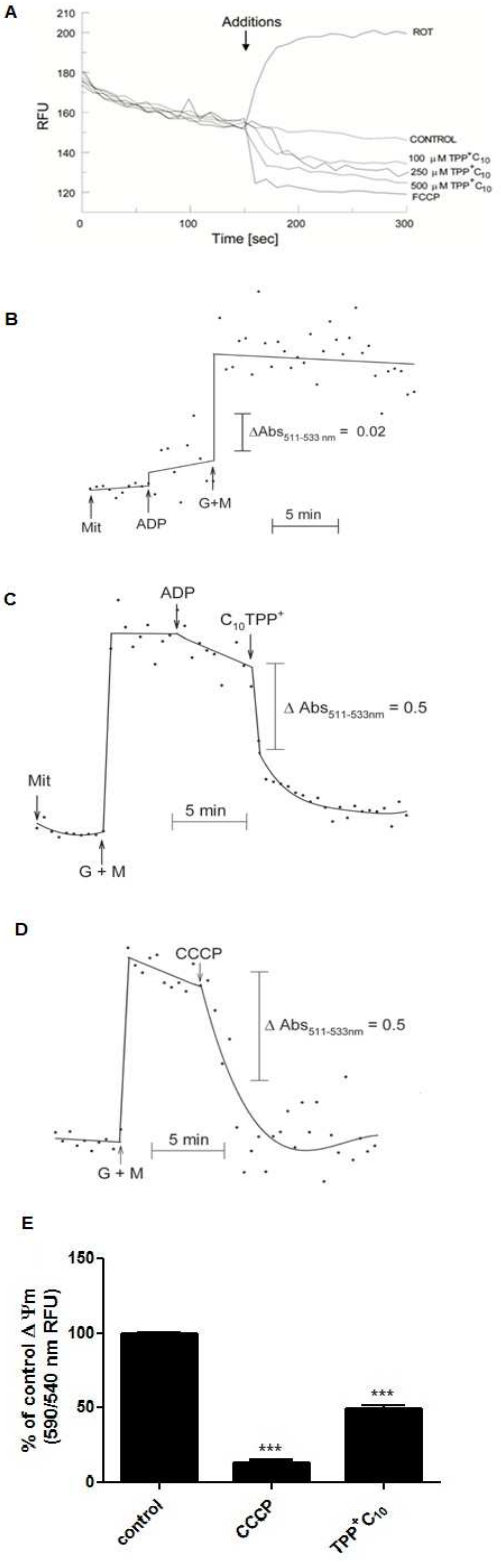
A
Additions
ROT
CONTROL
100 μM TPP+C10
250 μM TPP+C10
500 μM TPP+C10
FCCP
RFU
Time [sec]
B
ΔAbs511-533 nm = 0.02
Mit
ADP
G+M
5 min
C
ADP
C10TPP+
Δ Abs511-533nm = 0.5
Mit
G + M
5 min
D
CCCP
Δ Abs511-533nm = 0.5
G + M
5 min
E
% of control ΔΨm (590/540 nm RFU)
control
CCCP
TPP+C10
***
***

Figure 4

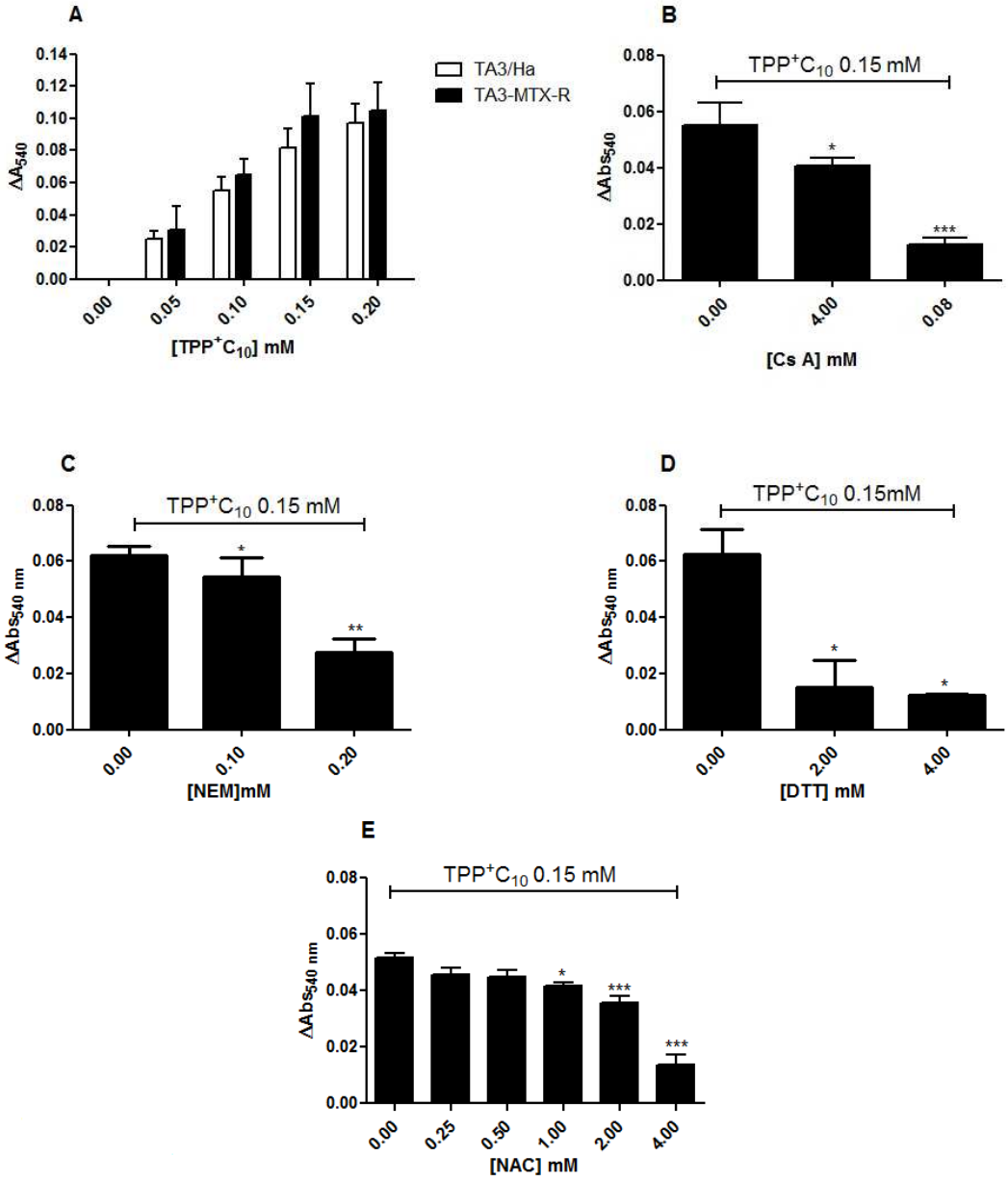
A
TA3/Ha
TA3-MTX-R
ΔA540
[TPP+C10] mM
B
TPP+C10 0.15 mM
ΔAbs540
[Cs A] mM
C
TPP+C10 0.15 mM
ΔAbs540 nm
[NEM]mM
D
TPP+C10 0.15mM
ΔAbs540 nm
[DTT] mM
E
TPP+C10 0.15 mM
ΔAbs540 nm
[NAC] mM

Figure 5

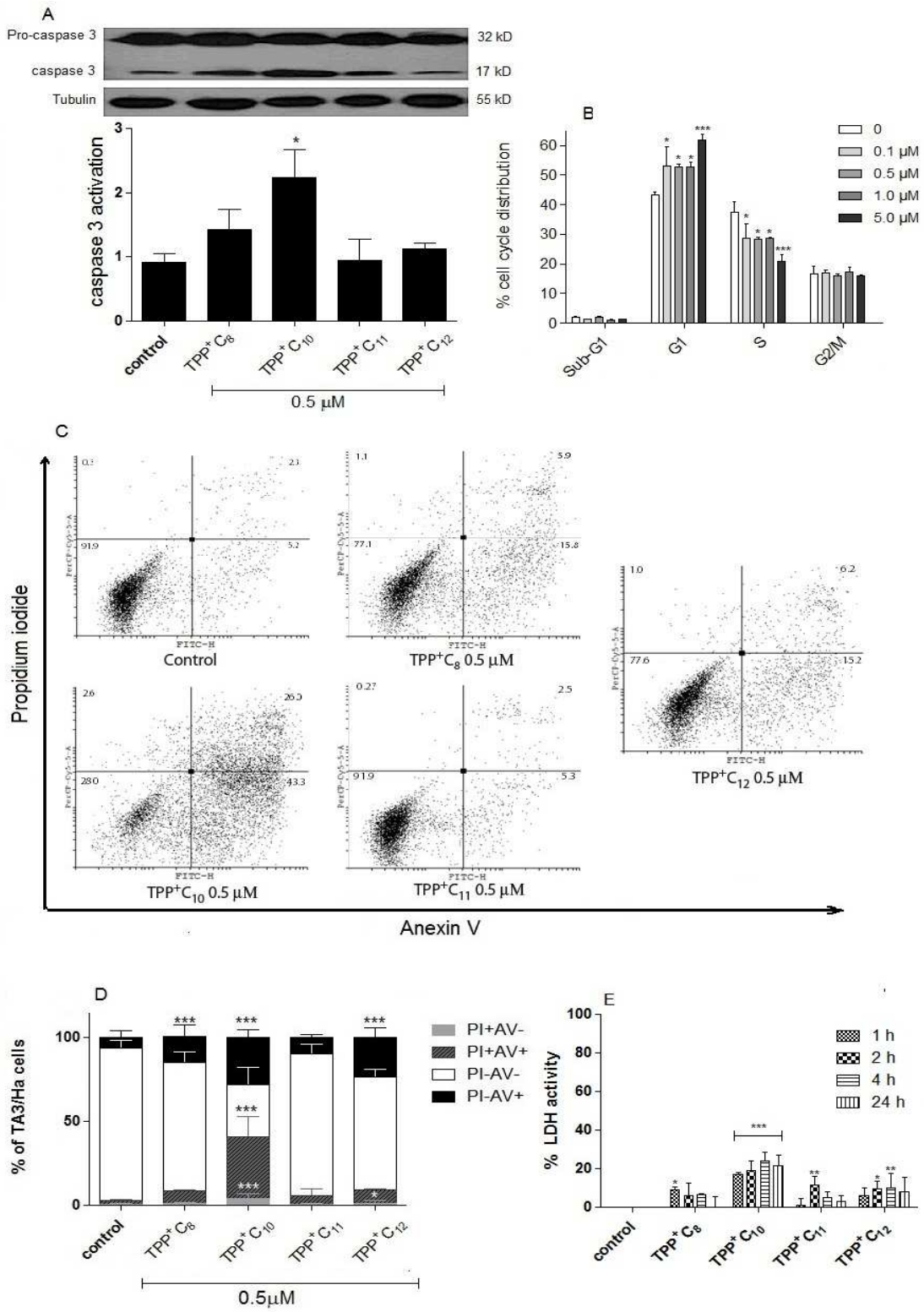
A
Pro-caspase 3
caspase 3
Tubulin
32 kD
17 kD
55 kD
caspase 3 activation
control
TPP+C8
TPP+C10
TPP+C11
TPP+C12
0.5 μM
B
% cell cycle distribution
Sub-G1
G1
S
G2/M
0
0.1 μM
0.5 μM
1.0 μM
5.0 μM
C
Propidium iodide
Anexin V
Control
TPP+C8 0.5 μM
TPP+C10 0.5 μM
TPP+C11 0.5 μM
TPP+C12 0.5 μM
D
% of TA3/Ha cells
PI+AV-
PI+AV+
PI-AV-
PI-AV+
0.5μM
E
% LDH activity
1 h
2 h
4 h
24 h

Figure 6

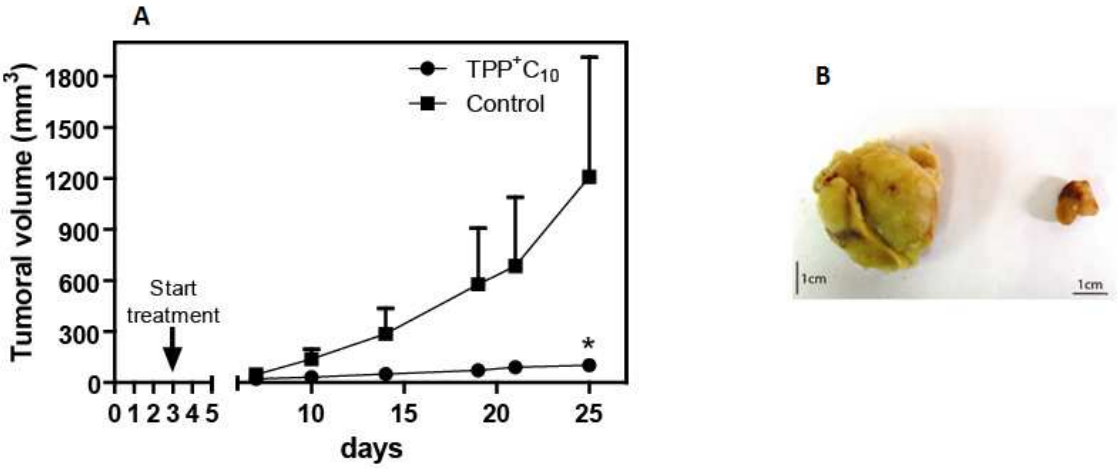
A
Tumoral volume (mm3)
1800
1500
1200
900
600
300
0
TPP+C10
Control
Start
treatment
*
0 1 2 3 4 5
10
15
20
25
days
B
1cm
1cm

Figure 7

TABLE OF CONTENTS GRAPHICS

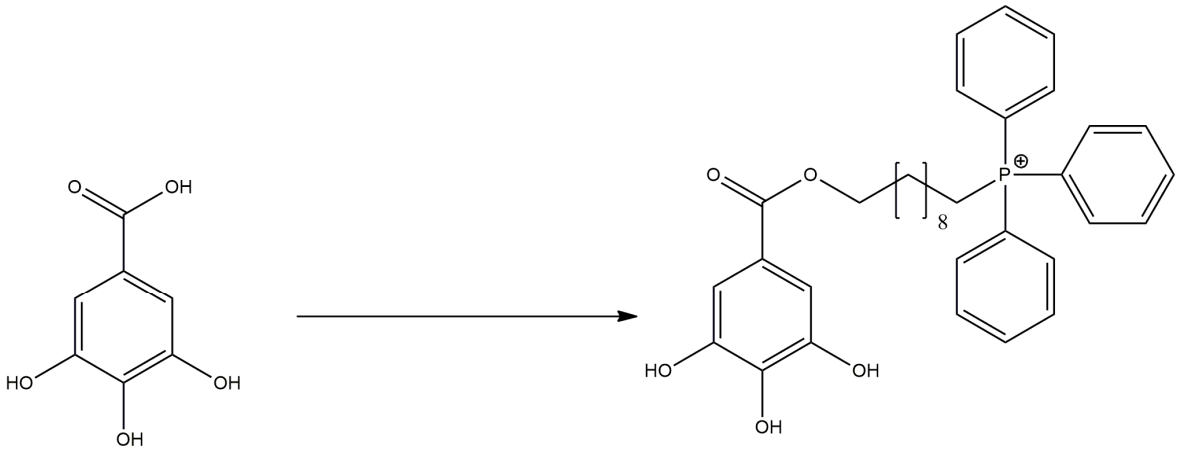

Gallic acid
IC_{50} TA3/Ha Cancer cell = 160 μM
IC_{50} MM3MG Normal cell > 200 μM

$TPP^{+}C_{10}$
IC_{50} TA3/Ha Cancer cell = 0.4 μM
IC_{50} MM3MG Normal cell = 7.1 μM